S1 Minimalist Analytical Solution

The analytical solution for the minimalist PHM is derived by equating supply (T_s^{phm}; Eqn. 1 of the article) and demand (T_s^{phm}; Eqns. 2-3 of the article) and solving for ψ_l^* as shown in Equation S1.

$$
\begin{aligned}
g_{sp} \cdot (\psi_s - \psi_l) &= \frac{\psi_{l,c} - \psi_l}{\psi_{l,c} - \psi_{l,o}} \cdot T_{ww} \\
\psi_l^* &= \frac{\psi_{l,c} - \psi_{l,o}}{T_{ww} - g_{sp} \cdot \left(\psi_{l,c} - \psi_{l,o}\right)} \cdot \left(\frac{T_{ww} \cdot \psi_{l,c}}{\psi_{l,c} - \psi_{l,o}} - g_{sp} \cdot \psi_s \right) \\
\psi_l^* &= \frac{T_{ww} \cdot \psi_{l,c} - g_{sp} \cdot \psi_s \cdot \left(\psi_{l,c} - \psi_{l,o}\right)}{T_{ww} - g_{sp} \cdot \left(\psi_{l,c} - \psi_{l,o}\right)} \\
\psi_l^* &= \frac{\frac{T_{ww} \cdot \psi_{l,c}}{g_{sp}} + \psi_s \cdot \left(\psi_{l,o} - \psi_{l,c}\right)}{\frac{T_{ww}}{g_{sp}} + \left(\psi_{l,o} - \psi_{l,c}\right)}
\end{aligned}
\tag{S1}
$$

Substituting ψ_l^* back into Equation 1 of the article yields the analytical solution for the minimalist PHM (Eqn. S2 and Eqn. 4 in the article). Algebraic manipulations shows that the solution is simply T_d^{phm} with an additional dependence on the ratio of atmospheric moisture demand and soil-plant conductance in the denominator.

$$
\begin{aligned}
T^{phm} &= g_{sp} \cdot (\psi_s - \psi_l^*) \\
&= g_{sp} \cdot \left(\psi_s - \frac{\frac{T_{ww} \cdot \psi_{l,c}}{g_{sp}} + \psi_s \cdot \left(\psi_{l,o} - \psi_{l,c}\right)}{\frac{T_{ww}}{g_{sp}} + \left(\psi_{l,o} - \psi_{l,c}\right)} \right) \\
&= g_{sp} \cdot \left(\frac{\psi_s \cdot \frac{T_{ww}}{g_{sp}} + \psi_s \cdot \left(\psi_{l,o} - \psi_{l,c}\right)}{\frac{T_{ww}}{g_{sp}} + \left(\psi_{l,o} - \psi_{l,c}\right)} - \frac{\frac{T_{ww} \cdot \psi_{l,c}}{g_{sp}} + \psi_s \cdot \left(\psi_{l,o} - \psi_{l,c}\right)}{\frac{T_{ww}}{g_{sp}} + \left(\psi_{l,o} - \psi_{l,c}\right)} \right) \\
&= T_{ww} \cdot \frac{\left(\psi_{l,c} - \psi_s\right)}{\left(\psi_{l,c} - \psi_{l,o}\right) - \frac{T_{ww}}{g_{sp}}}
\end{aligned}
\tag{S2}
$$

A key conclusion of this work relates to the nonlinearity in the PHM with respect to T_{ww}, even in the simplest case of the minimalist model. This nonlinearity can be shown formally by violating the superposition principle $T^{phm}\left(\psi_s, c_1 \cdot T_{ww,1} + c_2 \cdot T_{ww,2}\right) \neq c_1 \cdot T^{phm}\left(\psi_s, T_{ww,1}\right) + c_2 \cdot T^{phm}\left(\psi_s, T_{ww,2}\right)$. This is the fundamental difference between β and PHMs and results in the T_{ww}/g_{sp} term in the denominator of Equation S2.

S2 Additional LSM Results

S2.1 Soil Water Availability and Atmospheric Moisture Demand

The improved performance of PHMs during midday of July-August (Figs. 4c-d in the article) are explained by looking at the temporal breakdown of the well-watered transpiration (T_{ww}) and site data of soil water availability (Fig. S1). The T_{ww} is a proxy for stomata-regulated atmospheric moisture demand at the site and is the greatest from 10 AM to 3 PM during the later summer months. The measured volumetric water content shows water stress during the later summer months as well. Therefore, these diurnal results suggest that PHMs are most important during periods of high atmospheric moisture demand and low soil water availability.

S2.2 Fitting β Schemes

The three β transpiration downregulation schemes used in this work were 'calibrated' by fitting their respective parameters to the outputs of the calibrated LSM that uses a PHM scheme (the calibration process is detailed more extensively in section S5). The calibrated LSM outputs are relative transpiration, T/T_{ww}, for the sunlit and shaded big leaf (dots in Fig. S2e-f). We decided to avoid calibrating each LSM directly with a β scheme to the site data, and instead derive the β scheme from a fitted PHM scheme, because we wanted to ensure that any improvements resulting from PHM can be directly related to the ability of PHM to capture downregulation more realistically.

The single β scheme (β_s) has a Weibull curve (Eqn. 16 in the article) fit to the combined calibrated sunlit and shaded T/T_{ww} using nonlinear least squares in MATLAB. The fitted β_s parameter values for $\psi_{s,50}$ and b_s are -6.95 MPa and 2.54, respectively (shown in Fig. S2a-d in light gray). The two-leaf β scheme (β_{2L}) fits a β curve to the calibrated sunlit and shaded T/T_{ww} separately. The fitted β_{2L} parameter values for $\psi_{l,50}$ and b_l are -6.08 (-7.62) MPa and 2.12 (3.5) for the sunlit (shaded) big leaf (shown in Fig. S2a-d in dark gray). The reader is referred to section S6 for details of how these β curves are used in LSM calculations.

The 'dynamic β' scheme (β_{dyn}) was fit to the calibrated T/T_{ww} using a two-step process. First, the T/T_{ww} values were parsed into 10 bins covering the T_{ww} range for the sunlit and shaded big leaf separately and a single β curve was fit to each bin (shown by the black circles in Figure S2a-d). Second, a line was fit to the parameters $\psi_{s,50}$ and b_s as a function of T_{ww} shown by the red line and the corresponding linear equation in Figure S2a-d. Therefore, the parameters of β can dynamically change with the atmospheric moisture demand represented by T_{ww}. This is illustrated in Figure S2e-f by the isolines of β_{dyn} with respect to T_{ww} and closely match the color gradient of the calibrated T/T_{ww} values. The variation of β_{dyn} with respect to T_{ww} is well described by linear functions, with the exception of a slight noise in the shaded leaf b_s value, which is likely due to the clustering of T/T_{ww} values around 1 in wetter conditions in Figure S2f.

The β_{dyn} has great potential for parsimoniously representing the complexity of a PHM. The slope and intercepts of the β_{dyn} linear parameters for sunlit and shaded leaves are very similar making separate leaf fits unnecessary. Therefore, the complexity of the PHM can be represented by a 'dynamic β' with 4 total parameters (2 slope and 2 intercept), which is two more than the original β model as mentioned in the paper. A promising avenue of future work is to relate these four parameters to key plant hydraulic traits and soil parameters.

S2.3 RMSE Comparison of PHM and β Schemes

The improvements of the PHM scheme to the β_s and 'dynamic β' schemes are shown in terms of reduction in percent bias in Figure 4e-f. These results are corroborated by the change in root mean square error as shown in Figure S3. The RMSE results only differ from those based on reduction in percent bias in terms of improvements that are concentrated toward the highest T_{ww} periods, since that is where the highest magnitude errors occur.

S2.4 LSM Cumulative Energy and Carbon Budget Errors

To aid the interpretation of the LSM case study, we have also calculated the cumulative error compared to key measured fluxes at the US-Me2 site for the LSM run with five separate transpiration downregulation schemes (Table S1). Clearly, the PHM and β_{dyn} schemes provide the greatest improvement to evapotranspiration (ET) and gross primary productivity (GPP) with a 9% and 5% reduction in cumulative error, respectively, while differences in sensible heat flux (H), net radiation (R_{n}) and outgoing longwave radiative flux (L_{out}) appear less significant. Although they can be outweighted by energy balance closure errors in the flux tower data (up to 20%[1]), these improvements in percent bias (Fig. 4e-f) and root mean square error (Fig. S3) are consistent with our theoretical analysis of fundamental differences between β and a PHM under varying environmental conditions. Therefore, these errors may persist and grow under longer simulations and more variable environmental conditions.

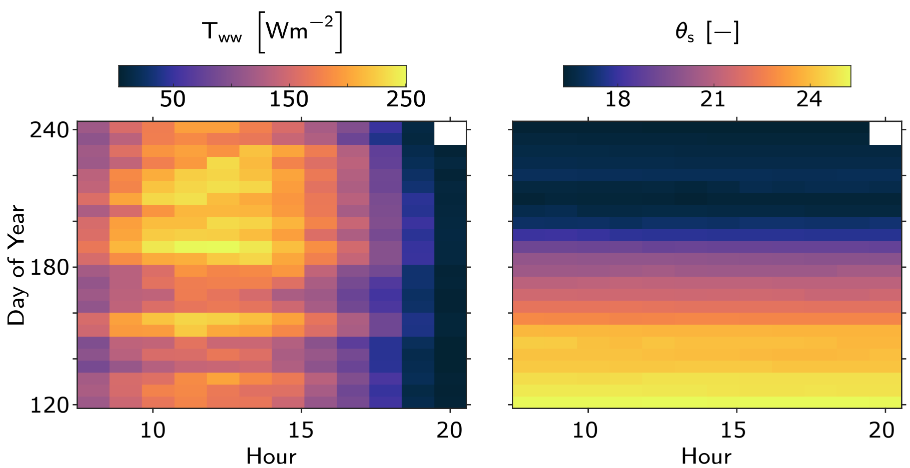

Figure S1. Left: Well-watered transpiration rate calculated form the LSM run with no transpiration downregulation. This is a proxy for the stomata-regulated atmospheric moisture demand. Right: Measured volumetric water content of soil at the US-Me2 site at 50 cm depth. The colors are the average value for the temporal bins for May-August 2013-2014.

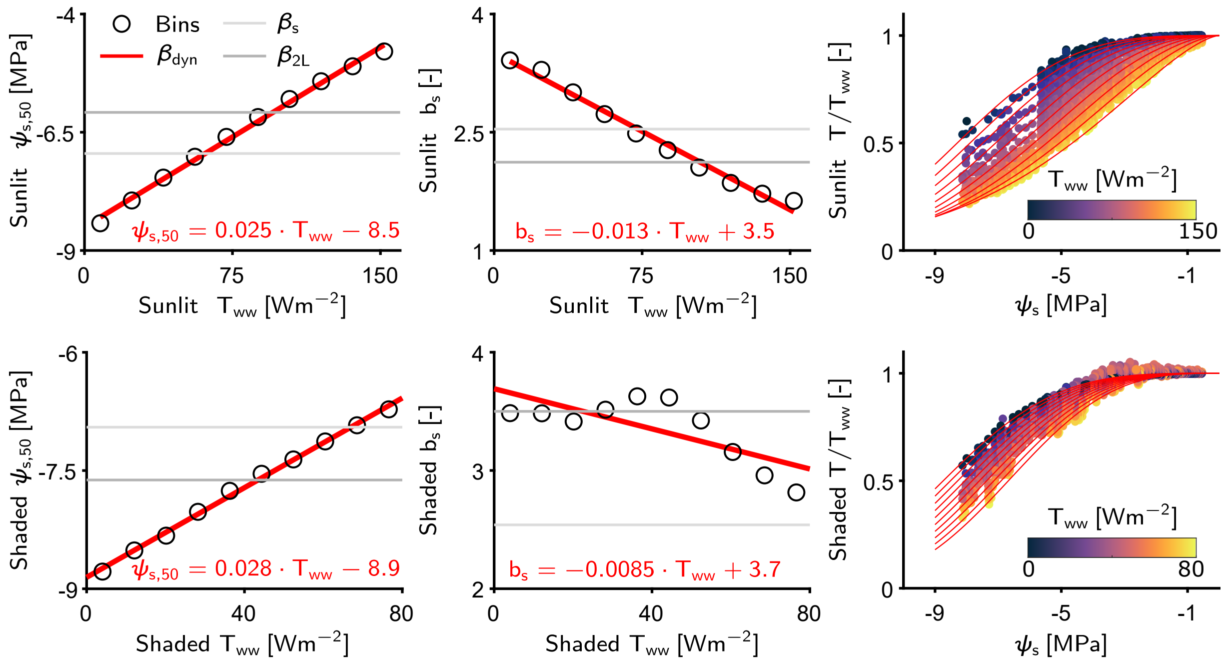

Figure S2. The 'dynamic β' (β_{dyn}) fits used for the sunlit (top row) and shaded big leaf (bottom row). The first column is the dependence of the soil water potential at 50% loss of stomatal conductance on well-watered transpiration T_{ww}. The second column is the dependence of the stomatal sensitivity parameter (b_s) to T_{ww}. The black circles are parameter values fit to relative transpiration (T/T_{ww}) binned over the range of T_{ww}. The linear relationship for both parameters is shown in red. The last column shows the relative transpiration outputs from the calibrated PHM with dot colors corresponding to T_{ww}. The red lines are the β_{dyn} model isolines at 10 values of T_{ww} (Equation 16 of the main article). These isolines clearly follow the color gradient of the PHM results indicating that β_{dyn} is able to capture the complexity of a PHM.

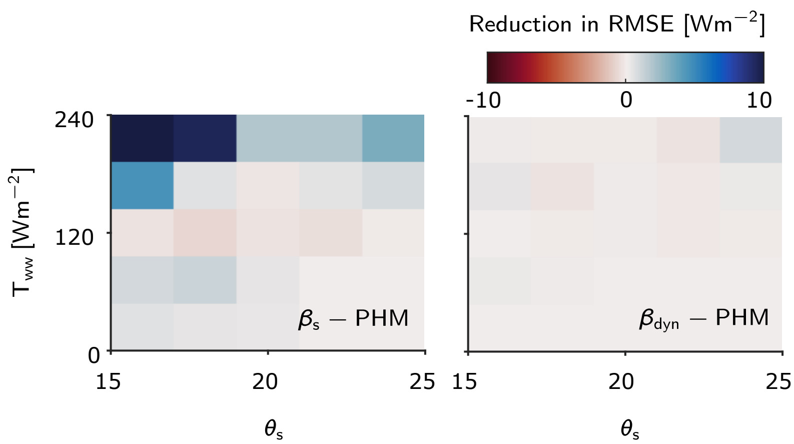

Figure S3. Analogous results to Figure 5e-f in the main text using root mean square error instead of percent bias as the performance metric. The differences in reduction of RMSE between the PHM and β_s scheme (left) and β_{dyn} scheme (right).

Table S1. Cumulative total for evapotranspiration (ET), gross primary productivity (GPP), sensible heat flux (H), net radiative flux (R_n), and longwave radiative flux (L_{out}) for Ameriflux Me2 data and 5 LSM simulations during high evaporative demand ($ET_{ww} > 150 W m^{-2}$) and low soil moisture (Volumetric soil water content < 0.2) for May-Aug 2013-2014. The surface energy fluxes are in units of cm H_2O and GPP is in units kg CO_2. The values in parentheses are the percent error compared to the observations.

	ET [cm]	**GPP [kg]**	**H [cm]**	**R_n [cm]**	**L_{out} [cm]**
WW	18.2 (34.4%)	1.7 (30.8%)	23.8 (-9.4%)	43.5 (-14.8%)	43.6 (10.4%)
PHM	13.6 (0.9%)	1.2 (-2.5%)	27.5 (4.7%)	42.6 (-16.4%)	44.5 (12.5%)
Beta	15 (10.8%)	1.4 (7%)	26.4 (0.6%)	42.9 (-15.9%)	44.2 (11.9%)
Beta2L	14.4 (6.9%)	1.3 (3.1%)	26.8 (2.2%)	42.8 (-16.1%)	44.3 (12.2%)
BetaDyn	13.6 (0.7%)	1.2 (-2.7%)	27.5 (4.8%)	42.6 (-16.4%)	44.5 (12.6%)

S3 Defining a Threshold for Transport-limitation

Quantifying the values of particular soil parameters and plant hydraulic traits that define a soil-plant system as transport-limited is an important avenue of future work. Figure 2 in the article illustrates clearly that, even in the minimalist model, there is a complex interplay of drivers that contribute to the differences between PHM and β and, in turn, if a system is transport- or supply-limited. However, the overall soil-plant conductance in the minimalist model seems to be the main control on transport-limitation and a $g_{sp} \approx 10^3\,Wm^{-2}MPa^{-1}$ appears to yield a supply-limited system (Fig. S4). The definition of transport-limitation is somewhat subjective as it depends on how much difference between PHM and β is considered acceptable.

Determining a threshold of transport-limitation for the complex PHM is even less clear given the additional parameters. Therefore, a sensitivity analysis was performed using the recent Variogram Analysis of the Response Surface (VARS) method[2] implemented with the VARSTOOL package in MATLAB[3]. The integrated difference in β and PHM-generated relative transpiration at high T_{ww} ($150\,Wm^{-2}$) normalized by the relative soil saturation of soil water stress (M_{dif}, Eqn. S3) was used as our metric to quantify the performance of each parameter set. The ranges and sensitivity scores for the 8 selected PHM parameters are shown in Table S2. The VARSTOOL analysis reveals that the maximum xylem-to-leaf conductance ($g_{xl,max}$) is the most sensitive parameter; thus, as maximum conductance in the plant decreases, a single β curve becomes increasingly ineffective at downregulating transpiration realistically. The next most sensitive parameters are $\psi_{x,50}$, b, $\psi_{l,50}$, b_l, and a, but they are of secondary importance. Lastly, the remaining two soil parameters, $\psi_{s,sat}$ and $g_{sx,max}$, were found to be the least sensitive parameters because transport-limitation from soil is primarily controlled by b.

$$M_{dif} = \frac{1}{T_{ww} \cdot (\theta_o - \theta_c)} \cdot \int_{\psi_s} T^{\beta}(\psi_s) - T^{phm}(\psi_s, T_{ww})\, d\psi_s \tag{S3}$$

Focusing on $g_{xl,max}$, we estimate a threshold for transport-limitation similar to the minimalist model. We do so by parsing the $g_{xl,max}$ range into 14 bins and sampling 5000 parameter sets from each bin (the 7 other parameters are sampled from their entire range in Table S2 for this analysis). The resulting sensitivity metrics were plotted for each bin in Figure S4. As $g_{xl,max}$ becomes lower ($g_{xl,max} < 10^3\ Wm^{-2}MPa^{-1}$) there is a tendency for the PHM results to diverge substantially from those of a single β curve. This threshold notably coincides with that predicted by the minimalist model. The large amount of spread is likely caused by the interactions amongst the other parameters. Further work must be done to create a more robust relationship based on measurable plant and soil hydraulic parameters.

Table S2. VARSTOOL results for plant hydraulics model based on 35,600 parameter sets created using Progressive Latin Hypercube Sampling and 200 STAR sampling centers. The IVARS50 is an integrated metric of sensitivity that accounts for correlation of nearby parameter values in the parameter space. The sources for each parameter are how we determined a realistic range to sample from.

Parameter	Description	Range	Units	IVARs50	Sources
$g_{xl,max}$	Max xylem-to-leaf conductance	$[10^{-10},10^{-3}]$	$\frac{m}{sMPa}$	$1.6e^{-3}$	[4,5]
$\psi_{x,50}$	Xylem water potential at 50% loss of conductance	[-0.1,-15]	MPa	$8.0e^{-4}$	[6–8]
b	Soil retention curve exponent	[2,14]	-	$1.5e^{-5}$	[9]
$\psi_{l,50}$	Leaf water potential at 50% loss of conductance	[-0.1,-15]	MPa	$3.5e^{-4}$	[4]
a	Xylem vulnerability curve shape parameter	[0.2,10]	-	$2.4e^{-4}$	[10]
b_l	Leaf vulnerability curve shape parameter	[0.2,5]	-	$1.0e^{-4}$	[10]
$g_{sx,max}$	Max soil-to-xylem conductance	$[10^{-2},10^{3}]$	$\frac{m}{sMPa}$	$3.0e^{-5}$	[4,11]
ψ_{sat}	Saturated soil water potential	$[10^{-3},10^{-2}]$	MPa	$3.2e^{-6}$	[9]

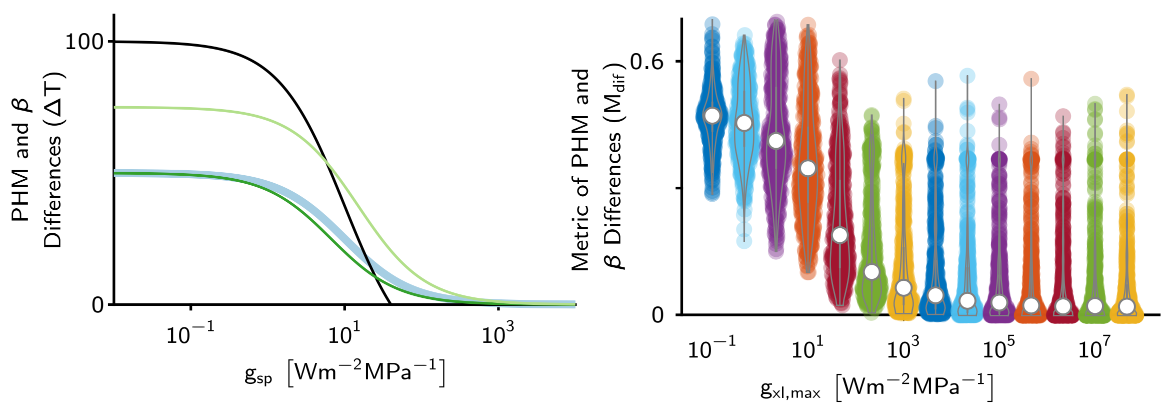

Figure S4. The control of soil-plant conductance (g_{sp}) on transport-limitation of a soil-plant system. Left: Differences in minimalist PHM and β as a function of overall soil-plant conductance. The thick blue line represents change in g_{sp} with three other drivers at baseline values (see Figure 2 in main article) while the thin lines represent 50% increase in ψ_s (black), T_{ww} (light green) and $\psi_{l,c} - \psi_{l,o}$ (dark green) compared to their baseline values. Right: Differences between a more complex formulation of PHM and β used in the LSM analysis with respect to maximum xylem-to-leaf conductance. The metric used integrates the difference between relative transpiration of β and PHM at a $T_{ww} = 150\,Wm^{-2}$ normalized by the range of soil water availability over which downregulation occurs (Eqn. S3).

S4 LSM Forcing Data

The LSM for the US-Me2 ponderosa pine site was forced with half-hourly atmospheric and subsurface measurements at the site. This site was specifically selected for the LSM case study based on its extensive subsurface soil moisture and temperature profiles as well as its separate measurements of photosynthetically active radiation (PAR) and near infrared radiation (NIR). The extensive soil moisture and temperature data and detailed shortwave radiation measurements were used as forcing for the LSM in lieu of one-dimensional mass and heat transfer equations and atmospheric radiation partitioning models. The main focus of this work was on the scalar transport of the LSM, so use of these measurements help reduce confounding errors from other model structures (although there would still be measurement errors).

The following atmospheric measurements from the Ameriflux US-Me2 dataset for May-August 2013-2014 were used to force the LSM: friction velocity (u^*), mean streamwise velocity ($\overline{u}$), air temperature (T_a), water vapor pressure (e_a), atmospheric pressure (P_{atm}), and CO_2 partial pressure (c_a). The radiative site measurements consisted of total incoming shortwave (S_{in}) and longwave radiation (L_{in}) as well as total and diffuse PAR. The LSM requires partitioning of shortwave radiation into PAR and NIR as well as direct beam and diffuse quantities. The diffuse incoming PAR ($S_{in,par,d}$) was measured at the site and the direct beam PAR ($S_{in,par,b}$) was calculated by the difference of total PAR ($S_{in,par}$) and diffuse PAR. Unfortunately, the site did not differentiate between direct beam ($S_{in,nir,b}$) and diffuse NIR ($S_{in,nir,d}$); therefore, total NIR was partitioned using the same ratio of direct and diffuse PAR at every time step. These detailed radiation measurements constrained the use of data from 2013-2014, as this was when they were most consistently available.

The subsurface moisture and temperature data was used to calculate the soil water availability of the root zone and the ground heat flux G at each time step. The G used to force the model was simply the thermopile measurements at 5 cm. In contrast, selecting a depth for the soil water content (θ_s) that would be representative of root-zone soil water availability was more difficult given there is minimal information at the US-Me2 site about the root structure. The US-Me2 site has θ_s measurements at 10, 20, 30, 50, 70, 100, 130, and 160 cm at multiple locations. To select a representative depth, we analyzed GPP deviations from the mean in terms of θ_s and vapor pressure deficit (D) at each depth (Fig. S5). All GPP values were studentized (i.e., mean subtracted and normalized by standard deviation) by hourly subsets for the period of May-August 2002-2014 to remove diurnal variation in flux magnitude and the median of these scores is plotted for each θ_s-D bin. The blue (red) values indicate lower (higher) than average GPP fluxes. As expected, measurements at each depth show lower values during water stress periods (low θ_s and high D). However, the ranges of θ_s experienced varies with depth, likely due to the combined effects of variable soil moisture profile, soil texture heterogeneity, and sensor inaccuracy. We selected the depth of 50 cm to use as our soil moisture forcing for two reasons: 1) there is a clear signal of GPP downregulation covering a wider range of soil moistures, and 2) a depth of 50 cm seems reasonable to represent the average moisture conditions when looking at meta-analyses of temperate coniferous forest root measurements[12].

A crucial consequence of using the subsurface inputs as model forcings is that it allowed the model time steps to be run in parallel. Typically, the model must be run sequentially since the subsurface models are partial differential equations in space (soil column) and time, and each time step relies on previous energy stored in the subsurface. The observations codify this temporal information, thereby allowing the LSM to run steady-state energy partitioning on top of the temporal dynamics of soil moisture and heat. Additionally, the LSM simulation was run only for time steps 24 hours after precipitation, since the model was not coded to handle canopy precipitation interception. Lastly, atmospheric stability effects were ignored for simplicity, as they add an additional layer of complexity to the solution scheme[13].

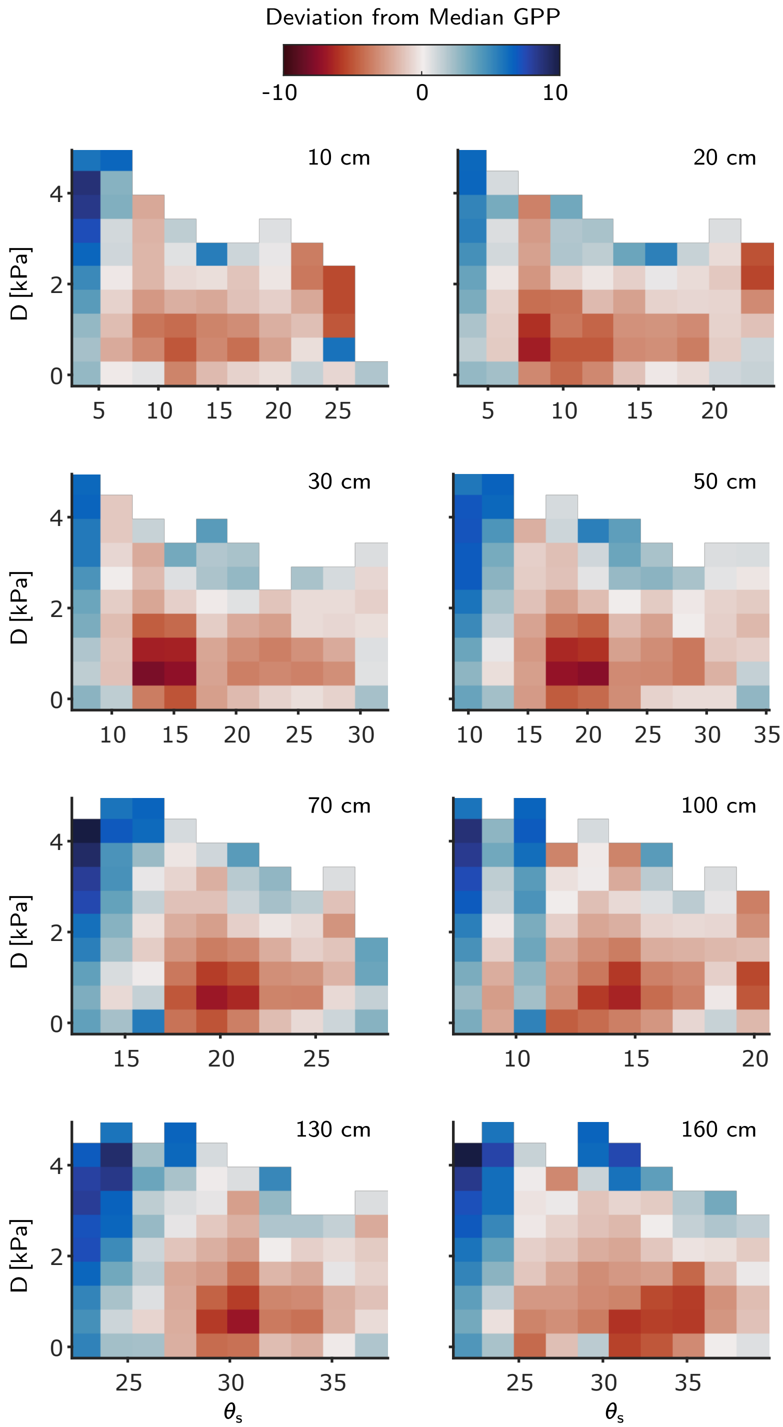

Figure S5. Median scores of the studentized gross primary productivity (GPP) measurements at the US-Me2 flux site for differing depth so soil water content θ_s measurements. The θ_s and vapor pressure deficit (D) measurements help identify water stress periods. The GPP data used are from May-August 2002-2014 and are studentized by their hourly subset to remove diurnal variations. Blue (red) in the plots is an indicator of decreased (increased) GPP from the mean value.

S5 LSM Calibration

The LSM was calibrated using a grid search of 13,600 parameter sets with 15 soil, plant and radiative parameters shown in Table S3. The parameters sets were created using Progressive Latin Hypercube Sampling available in the VARSTOOL package[3] in MATLAB. The 13,600 simulations were run for May-August 2013-2014 for the hours of 8 AM to 8 PM, excluding 24 hours following any precipitation event.

The best simulation was selected based on a performance metric evaluating evapotranspiration (ET), sensible heat flux (H), gross primary productivity (GPP) and net radiation (R_n) predictions. The performance metric (M_{cal}; Eqn. S4) consists of Taylor diagram statistics[14]: 1) the correlation coefficient (R), 2) the centered root mean square error ($CRMSE$), and 3) the variance (σ). The percent bias (P_b) was also added to the metric to account for the mean difference in simulation and observation. Each index i in the summation of Equation S4 represents a different flux which are combined to form a single metric.

$$M_{cal} = \sum_{i}^{n} \frac{R_i}{max(R)} - CRMSE_i - P_{b,i} - \frac{\Delta\sigma_i}{max(\Delta\sigma)} \tag{S4}$$

The three best fits from the VARSTOOL grid search (VT1-VT3) were selected based on the metric. The best VARSTOOL parameter set (VT1) was further adjusted by reducing $g_{xl,max}$ by 60% to reduce biases found in representing ET. This is the calibrated parameter set used in the article and is labeled 'Best Fit' in the following figures. The metric value of all LSM runs are shown in Figure S6 in terms of R and $CRMSE$. The selected best parameter sets trade-off improvements between ET, H, GPP, and R_n. The outgoing longwave (L_{out}) and shortwave radiation (S_{out}) were ignored as including them in the metric had minimal effect. The 'Best Fit' (red x) provides clear improvement to the R and $CRMSE$ compared to VT1-VT3 for ET. The median diurnal fluxes for the observations and best fit LSM runs during May-June (Fig. S7) and July-August (Fig. S8) reveal the largest performance differences between parameter sets are for ET and GPP predictions. The over-prediction of ET during soil water stress (Fig. S8) informed our decision to create the 'Best Fit' parameter set by reducing $g_{xl,max}$ to correct the bias. This manual adjustment also provides slight performance increases to the second order statistics of all fluxes illustrated in the Taylor diagram[14] in Figure S9.

The 'Best Fit' parameters set fit the ET observations well, but, as illustrated in Figure 4e of the article, the PHM downregulation scheme is not perfect as there are T_{ww}-θ_s bins where the β_s scheme performs the best. Looking at the P_b statistic for β_s, PHM and well-watered LSM runs in Figure S10, we see there are two primary reasons for β_s having the best performance for particular bins (highlighted in red): 1) the well-watered scheme is nearly unbiased so any downregulation will bias the result, and 2) the PHM over-regulates for these lower T_{ww} bins. For both situations, β_s downregulates less because it is fit to the mean behavior of the PHM, resulting in a better result. Therefore, the β_s is really just causing less bias in areas where the PHM performs poorly due to our fitting assumptions. The results in Figure S10 indicate that greater attention in the calibration process should be paid to the lower T_{ww} time steps to help correct these errors.

Table S3. The calibration parameters for the LSM with PHM downregulation scheme. The parameter ranges was used to create 13,600 parameters sets that were each run in the LSM. The calibrated value was selected based a performance metric (Eqn. S4) and additional adjustment in the above text. These values were used to run the LSM with PHM downregulation in the main article.

Parameter	Description	Range	Units	Calibrated Value
K_{sap}	Sapwood hydraulic conductivity	[10^{-7},10^{-2}]	kg m^{-1} s^{-1} MPa^{-1}	$9.3e^{-4}$
$\psi_{x,50}$	Xylem water potential at 50% loss of conductance	[-0.1,-15]	MPa	-2.3
a	Xylem vulnerability curve shape parameter	[0.2,10]	-	0.3
$\psi_{l,50}$	Leaf water potential at 50% loss of conductance	[-0.1,-15]	MPa	-9.9
b_l	Leaf vulnerability curve shape parameter	[0.2,5]	-	3.4
b	Soil retention curve exponent	[2,14]	-	5.1
$\psi_{s,sat}$	Saturated soil water potential	[10^{-3},10^{-2}]	MPa	$9.9e^{-3}$
$K_{s,sat}$	Saturated soil hydraulic conductivity	[0.01,20]	m d^{-1}	10
θ_i	Incipient soil water content for restricting bare soil evaporation	[0,0.57]	-	0.57
g_1	Medlyn Slope Parameter	[0.5,5]	$kPa^{0.5}$	0.9
$V_{max,25}$	Max Rubisco-limited carboxylation rate	[5,200]	μmol CO_2 m^{-2} s^{-1}	122
LAI	Leaf area index	[1.5,4]	m^{-2} LA m^{-2} GA	3.2
$\alpha_{l,par}$	Leaf reflectance to PAR	[0.5,1]	-	0.74
$\alpha_{l,nir}$	Leaf reflectance to NIR	[0,0.6]	-	0.43
χ_l	Leaf angle distribution parameter	[-0.4,0.6]	-	0.11

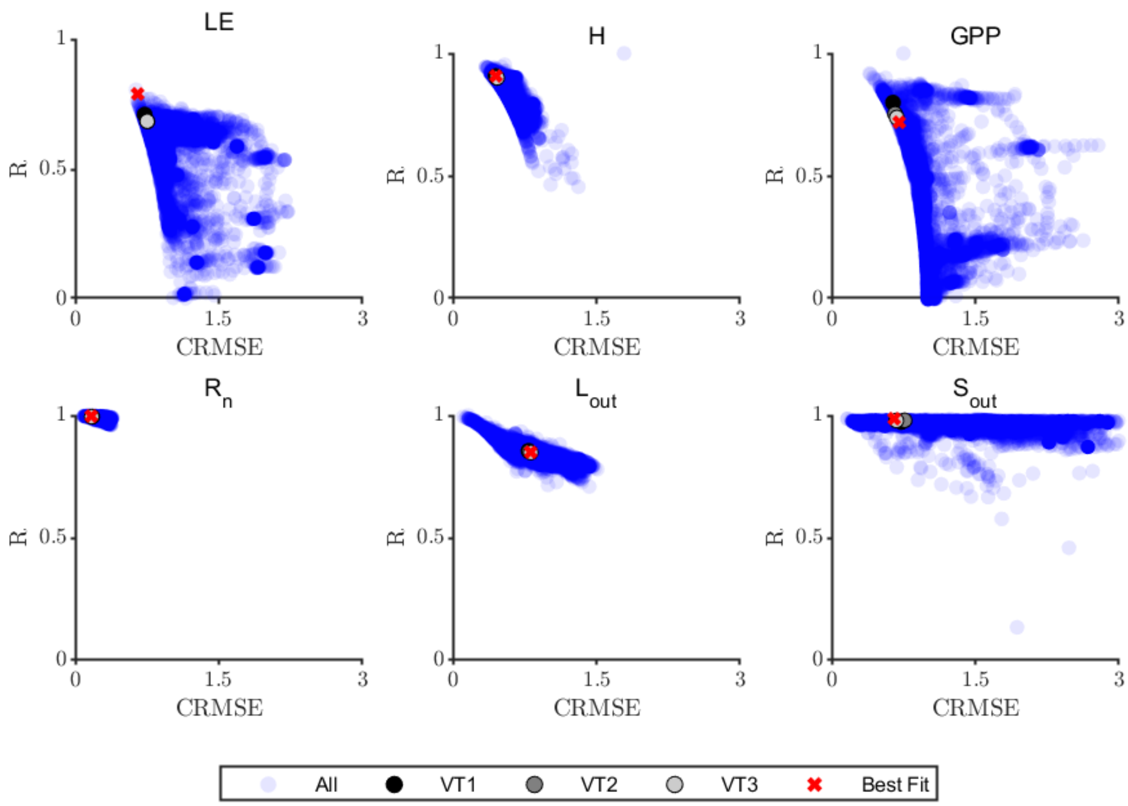

Figure S6. Centered root mean square error (CRMSE) and correlation (R) statistics for the LSM with PHM downregulation scheme for 13,600 parameters sets. An ideal score would be R = 1 and CRMSE = 0. The best fits from the VARSTOOL-created parameters sets, labelled VT1-VT3, are based on the metric in Equation S4, while a manual adjustment to VT1 was used to create the overall Best Fit used in the main article.

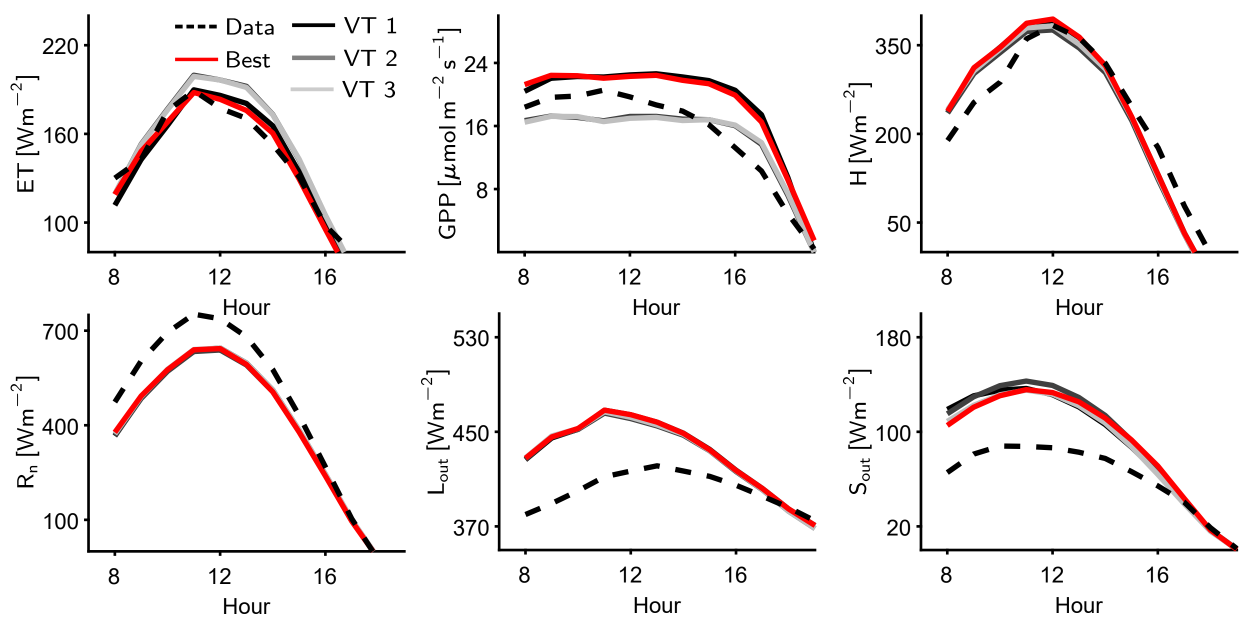

Figure S7. The median diurnal fluxes for May-June 2013-2014 for the three best VARSTOOL parameter sets (VT1-VT3) and the best overall calibrated fit (red) compared to the US-Me2 flux data for evapotranspiration (ET), gross primary productivity (GPP), sensible heat flux (H), net radiation (R_n), outgoing longwave radiation (L_{out}) and outgoing shortwave radiation (S_{out}).

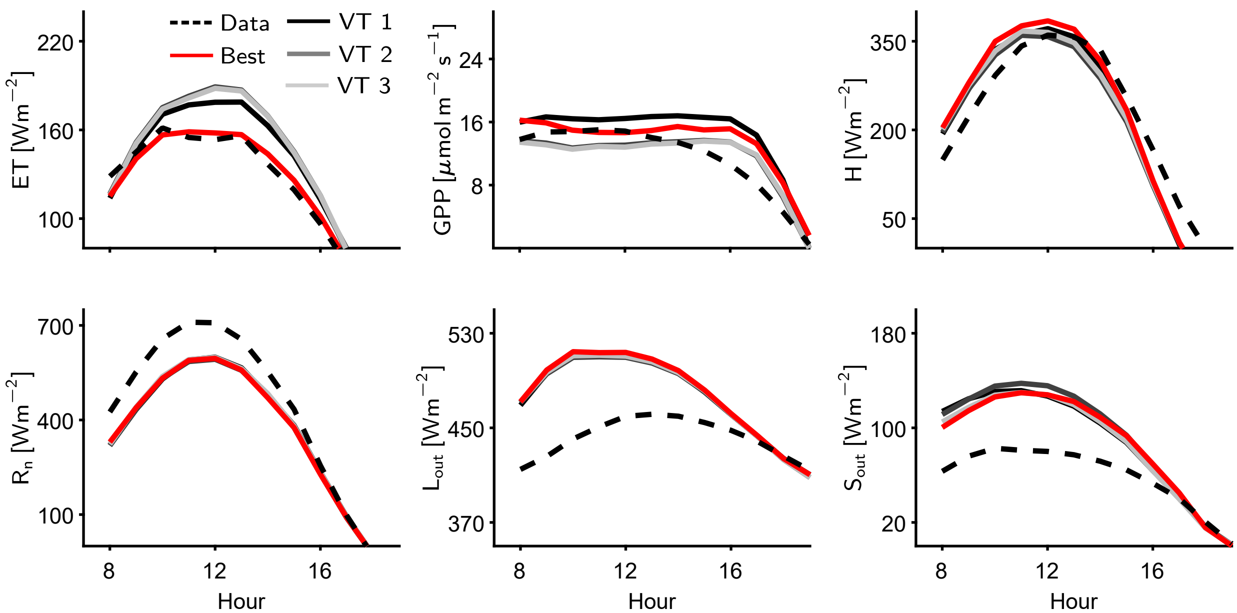

Figure S8. Same as Figure S7 for July-August 2013-2014 where there is soil water stress.

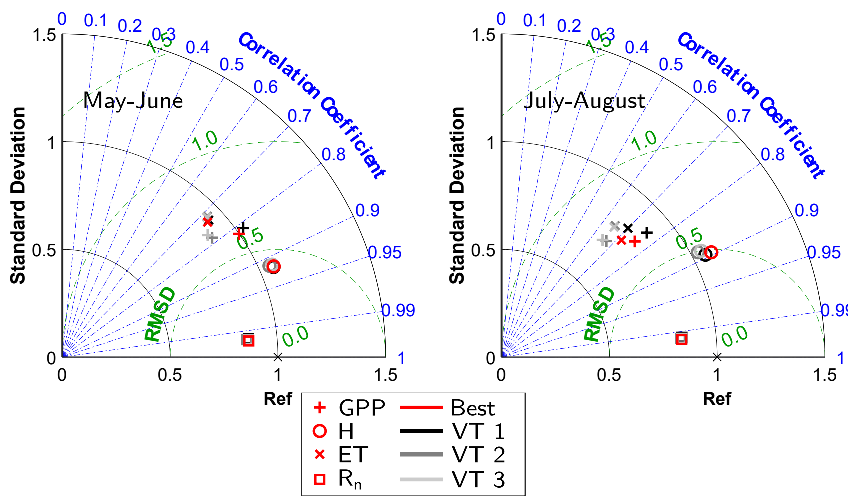

Figure S9. The Taylor diagrams for May-June 2013-2014 (left) and July-August 2013-2014 (right) for the three best VARSTOOL parameter sets (VT1-VT3) and the best overall calibrated fit (red) compared to the US-Me2 flux data for Evapotranspiration (ET), gross primary productivity (GPP), sensible heat flux (H), net radiation (R_n), outgoing longwave radiation (L_{out}) and outgoing shortwave radiation (S_{out}).

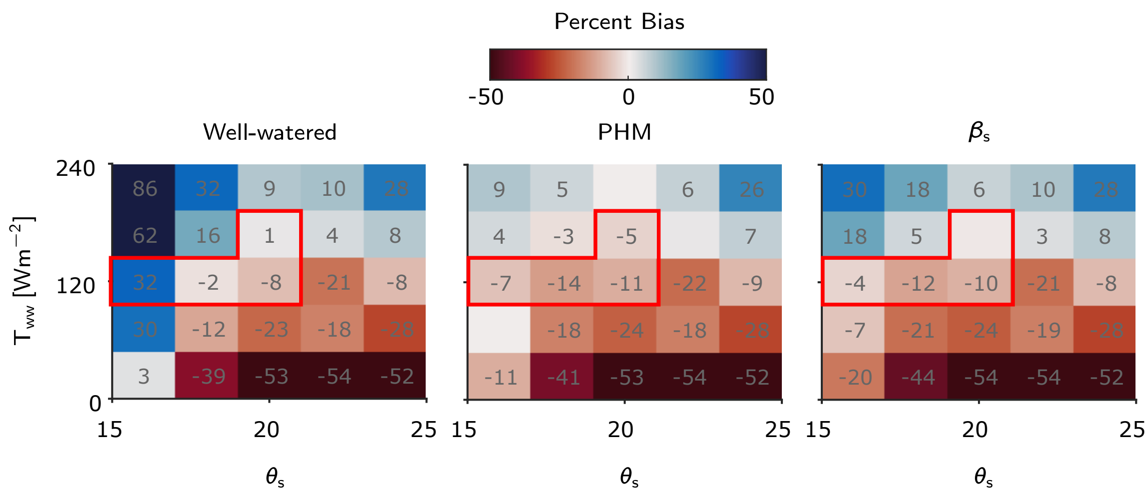

Figure S10. The percent bias (P_b) of the LSM with well-watered, PHM and β_s downregulation schemes compared to ET observations at the US-Me2 flux tower site. The P_b is broken down by well-watered transpiration T_{ww} and volumetric soil water content (θ_s) as in Figure 4e-f of the main article. The gray numbers give the exact P_b value for each bin while the red outline highlights the primary bins where β_s appears to outperform the PHM in Figure 4e of the main article. See text for explanation.

S6 LSM Description

This section lays out the land surface model (LSM) coded in MATLAB used for the analysis of the US-Me2 ponderosa pine Ameriflux site. The model is a two big leaf, dual source model[15] following closely the formulation laid out in the Community Land Model version 5[16] with key modifications. The general model structure for scalar transport is shown in Figure S11 with the main modules highlighted. Here, module refers to a smaller model within the overall LSM, e.g., the Plant Hydraulics Model (PHM). The purpose of this LSM is to compare the scalar transport (temperature, water vapor, and carbon transport) scheme using PHM and empirical (β) transpiration downregulation schemes; therefore, the model is simplified to be forced at the boundaries by incoming radiation, air scalar concentrations as well as soil water availability and heat flux. We are exploring the LSM component only during the growing season, so nutrient cycling, plant demographics, snow dynamics, and phenology components—common in terrestrial biosphere models like CLM— are ignored. This section is organized by the energy balance, radiative transfer, scalar transport, transpiration downregulation, and solution schemes.

We adopt a slight modification in terminology within this LSM description section. In the main text and other sections of this supplement, the transpiration flux is represented by the variable T; however, temperature is very prevalent in the LSM equations and is traditionally represented by T. To avoid confusion and be consistent with the conservation of energy in the LSM, we elect to represent transpiration in energy flux units (Wm^{-2}) and represent it with the variable for latent heat flux from the canopy (LE_l), where the subscript represents the big leaf approximation. Similarly the bare soil evaporation is represented (LE_g), where the subscript represents the ground. Thus, the latent heat flux (LE) is the sum of canopy and ground latent heat fluxes, which is simply evapotranspiration (ET) in energy units. The notation frees up the variable T to represent temperature.

S6.1 LSM Energy Balance

The energy balance of the soil-plant-atmosphere for the two big leaf, dual source LSM is shown by Equation S5. The net radiation (R_n) of the soil plant system is the difference of the incoming and outgoing shortwave (S_{in} and S_{out}, respectively) and longwave (L_{in} and L_{out}, respectively) radiation, i.e., the radiation absorbed by the soil-plant system. This absorbed radiation is available for sensible (H), latent (LE), ground heat flux (G) and storage (not included in this formulation). We assume here one-dimensional (vertical), steady-state energy transport (no energy storage) common in many LSMs. The dynamics in model outputs are controlled by the change in the forcing data. The steady-state simplification turns the solution from a numerical integration of a partial differential equation to numerical solutions of nonlinear equations and allows parallelization in computation.

$$R_n = S_{in} - S_{out} + L_{in} - L_{out} = H + LE + G \tag{S5}$$

The 'dual source' and 'two big leaf' descriptors indicate how the overall energy balance is broken up into smaller components. The dual source LSM structure means the surface is partitioned into plant canopy and ground components as sources of scalars (illustrated in Fig. S11). Additionally, we elect the two-layer form of the dual source structure, similar to

CLM v5[16], where both canopy and soil interact with a canopy airspace (Fig. S11), which, in turn, interacts with the atmosphere above the canopy. The two big leaf approximation further partitions the canopy component into a sunlit and shaded big leaf approximation representing the integrated fluxes of all sunlit and shaded leaves.

Before diving further into the energy balance of these LSM components, it is important to define some notation rules for the equations in this section that will clearly delineate the model structure. The notation rules for this LSM structure are as follows: 1) a subscript of 'l' or 'g' indicates canopy/big leaf or ground fluxes, respectively, 2) an additional subscript following 'l' such as 'sl' or 'sh' indicates the sunlit or shaded big leaf component of the canopy flux, 3) the index 'k' in lieu of 'sl' or 'sh' refers to both sunlit and shaded big leaves, 4) shortwave radiation terms have an additional subscript 'par' or 'nir', identifying the specific radiation band, i.e., whether it is photosynthetically active radiation (PAR) or near infrared radiation (NIR), and 5) a single subscript 'Λ' in lieu of 'par' or 'nir' refers to both bands.

Using the above conventions, Equation S5 can then be further broken down into three smaller balances for the sunlit big leaf (Eqn. S6), shaded big leaf (Eqn. S7), and the soil or ground (Eqn. S8). Balancing each of these equations separately is equivalent to balancing the overall energy budget in Equation S5. Furthermore, each total flux (Eqn. S5) requires consistency between model components as shown in Equations S9-S12.

$$R_{n,l,sl} = S_{l,sl,par} + S_{l,sl,nir} + L_{l,sl} = H_{l,sl} + LE_{l,sl} \tag{S6}$$

$$R_{n,l,sh} = S_{l,sh,par} + S_{l,sh,nir} + L_{l,sh} = H_{l,sh} + LE_{l,sh} \tag{S7}$$

$$R_{n,g} = S_{g,par} + S_{g,nir} + L_g = H_g + LE_g + G_g \tag{S8}$$

$$R_n = R_{n,l,sl} + R_{n,l,sh} + R_{n,g} = R_{n,l,k} + R_{n,g} \tag{S9}$$

$$H = H_{l,sl} + H_{l,sh} + H_g = H_{l,k} + H_g \tag{S10}$$

$$LE = LE_{l,sl} + LE_{l,sh} + LE_g = LE_{l,k} + LE_g \tag{S11}$$

$$G = G_g \tag{S12}$$

S6.2 Radiative Transfer

The radiative transfer model was forced with incoming PAR, NIR and longwave radiation based on site measurements (see section S4 for details). Here we discuss the separate shortwave and longwave radiative transfer models.

S6.2.1 Shortwave Radiative Transfer

We use the Goudriaan and van Laar (GvL) model[17] to estimate shortwave radiative transfer in lieu of the two-stream approximation[16,18] used in CLM v5. Both approaches are two-stream models that focus on the upward and downward net fluxes of diffuse radiation with single scattering[13]. However, the GvL model yields simpler analytical forms and is used in other TBMs such as CABLE[19]. The reader is referred to[13,17] for detailed derivation of the model. Shortwave radiation is partitioned into direct beam, scattered beam, and diffuse components of PAR and NIR. The two big leaf assumption also requires assuming that diffuse leaves only receive scattered beam and diffuse radiation, while sunlit leaves receive the same as well as direct beam radiation[13,16,20].

The total canopy shortwave radiation absorption $S_{l,\Lambda}$ is given by Equation S13. This values must be partitioned appropriately between the sunlit and shaded big leaf. For ease of calculation and completeness, the sunlit leaf shortwave radiation absorption ($S_{l,sl,\Lambda}$, Eqn. S14) is partitioned into direct beam ($S_{l,sl,\Lambda,b}$, Eqn. S15), diffuse ($S_{l,sl,\Lambda,d}$, Eqn. S16), and scattered direct beam ($S_{l,sl,\Lambda,sb}$, Eqn. S17) components following[20]. The shaded leaf shortwave absorption ($S_{l,sh,\Lambda}$, Eqn. S18) is simply the difference of total canopy absorption and sunlit leaf absorption, although analogous forms of the sunlit equations (Eqns. S15-S17) can also be used[20].

$$S_{l,\Lambda} = \left(1-\rho'_{l,\Lambda,b}\right) S_{in,\Lambda,b} \left(1-\exp[-K'_{b,\Lambda} \cdot LAI]\right) + \left(1-\rho'_{l,\Lambda,d}\right) S_{in,\Lambda,d} \left(1-\exp[-K'_{d,\Lambda} \cdot LAI]\right) \tag{S13}$$

$$S_{l,sl,\Lambda} = S_{l,sl,\Lambda,b} + S_{l,sl,\Lambda,d} + S_{l,sl,\Lambda,sb} \tag{S14}$$

$$S_{l,sl,\Lambda,b} = S_{in,\Lambda,b} \cdot \alpha_{l,\Lambda} \cdot (1-\exp[-K_b \cdot LAI]) \tag{S15}$$

$$S_{l,sl,\Lambda,d} = S_{in,\Lambda,d} \cdot (1-\rho'_{l,\Lambda,d}) \cdot (1-\exp[-(K'_{d,\Lambda}+K_b) \cdot LAI]) \cdot \frac{K'_{d,\Lambda}}{K'_{d,\Lambda}+K_b} \tag{S16}$$

$$S_{l,sl,\Lambda,sb} = S_{in,\Lambda,b} \cdot ((1-\rho'_{l,\Lambda,b}) \cdot (1-\exp[-(K'_{b,\Lambda}+K_b) \cdot LAI]) \cdot \frac{K'_{b,\Lambda}}{K'_{b,\Lambda}+K_b} + \alpha_{l,\Lambda} \cdot (1-\exp[-2K_b \cdot LAI])/2) \tag{S17}$$

$$S_{l,sh,\Lambda} = S_{l,\Lambda} - S_{l,sl,\Lambda} \tag{S18}$$

These radiative transfer equations rely on four essential parameters in the GvL model for shortwave radiative transfer: the direct (K_b) and diffuse extinction coefficients (K_d) and the direct ($\rho'_{l,b}$) and diffuse canopy reflectance coefficients ($\rho'_{l,d}$). The K_b value is calculated by dividing the mean leaf angle ($G(Z)$) by the projection of sunlight onto a horizontal surface (Eqn. S19), where Z is the sun zenith angle. The K_b value will change throughout the day as the sun moves across the sky since the angle of incidence with respect to leaf angles will vary. The function $G(Z)$ is known as the 'Ross-Goudriaan' function (Eqns. S20-S22), which depends on a parameter, χ_l, that describes the leaf angle distribution's deviation from a spherical (i.e., random) distribution. As mentioned in section S4, we calibrated χ_l to vary between -0.4 and 0.6.

$$K_b = \frac{G(Z)}{\cos(Z)} \tag{S19}$$

$$G(Z) = \phi_1 + \phi_2 \cos(Z) \tag{S20}$$

$$\phi_1 = 0.5 - 0.633\chi_l - 0.33\chi_l^2 \tag{S21}$$

$$\phi_2 = 0.877\,(1-2\phi_1) \tag{S22}$$

The diffuse radiation extinction coefficient, K_d, is calculated by integrating the direct beam transmissivity ($\tau_{l,b}$ shown in Eqn. S23) over every solid angle of the hemisphere (Eqn. S24) and then inverting the transmissivity law (Eqn. S25). The transmissivity describes the attenuation of the percent of radiation that makes it through the canopy to the soil as a function of distance from the canopy, through an exponential function.

$$\tau_{l,b} = \exp\left(-K_b \cdot LAI\right) \tag{S23}$$

$$\tau_{l,d} = \int_0^{\pi/2} \tau_{l,b} \cdot \cos Z \cdot \sin Z dZ \tag{S24}$$

$$K_d = \frac{-\ln \tau_{l,d}}{LAI} \tag{S25}$$

The GvL model has fewer equations than the CLM v5 two-stream approximation due to several simplifying assumptions. First, the single scattering of radiation can be accounted for in the extinction coefficients (K_b and K_d) simply by multiplying by the square root of leaf absorption (α_l)[17]. The extinction coefficients accounting for single-scattering are shown in Equations S26-S27. Second, leaf transmissivity and reflectance are assumed identical—a reasonable assumption for green canopies[17]—allowing derivation of simplified relationships for direct beam ($\rho_{l,b}$, Eqn. S28) and diffuse canopy reflectance ($\rho_{l,d}$, Eqn. S29) based on idealized reflectance of horizontal leaves ($\rho_{l,h}$, Eqn. S30). Readers are referred to[17,21] for further details on these assumptions.

$$K'_{b,\Lambda} = \sqrt{\alpha_{l,\Lambda}} \cdot K_b \tag{S26}$$

$$K'_{d,\Lambda} = \sqrt{\alpha_{l,\Lambda}} \cdot K_d \tag{S27}$$

$$\rho_{l,b} = \frac{2K_b}{K_b + K_d} \rho_{l,h} \tag{S28}$$

$$\rho_{l,d} = \int_0^{\pi/2} 2 \cdot \rho_{l,b} \cdot \cos Z \cdot \sin Z dZ \tag{S29}$$

$$\rho_{l,h} = \frac{1 - \sqrt{\alpha_{l,\Lambda}}}{1 + \sqrt{\alpha_{l,\Lambda}}} \tag{S30}$$

The above canopy reflectance equations were derived for infinitely deep canopies. To account for the ground reflectance (ρ_g), the approximations in Equations S31-S32 are used. These approximations assume radiation travels through the canopy, reflects off the soil according to ρ_g, and travels back up through the canopy (hence the factor of 2).

$$\rho'_{l,\Lambda,b} = \rho_{l,b} + \left(\rho_g - \rho_{l,b}\right) \exp(-2K'_b LAI) \tag{S31}$$

$$\rho'_{l,\Lambda,d} = \rho_{l,d} + \left(\rho_g - \rho_{l,b}\right) \exp(-2K'_d LAI) \tag{S32}$$

S6.2.2 Longwave Radiative Transfer

The longwave radiative transfer model follows the method laid out in[22], which is derived assuming exponential extinction of longwave radiation through the plant canopy. The net absorbed longwave radiation ($L_{l,k}$) is given by Equation S33, which depends on the sunlit and shaded leaf temperature ($T_{l,k}$), ground temperature (T_g), fraction of longwave radiation absorbed by the canopy (δ_l, Eqn. S34), the sunlit and shaded leaf fraction (F_k), and the Stefan-Boltzmann constant (σ). As mentioned previously, k is used to indicate that the equations are identical for sunlit or shaded big leaves.

$$L_{l,k} = \left(L_{in} - 2\sigma T_{l,k}^4 + \sigma T_g^4\right) \cdot \delta_l \cdot F_k \tag{S33}$$

$$\delta_l = 1 - \exp(-LAI) \tag{S34}$$

$$F_{k=1} = F_{sl} = \frac{1 - \exp(-K_b \cdot LAI)}{K_b \cdot LAI} \tag{S35}$$

$$F_{k=2} = F_{sh} = 1 - F_{sl} \tag{S36}$$

S6.3 Scalar Transport

Scalar transport for this LSM consists of prognostic equations for latent heat flux (LE), sensible heat flux (H) and gross primary productivity (GPP). The conserved quantities are mass of H_2O and CO_2 as well as enthalpy ($c_p \cdot T$). The states of the soil-plant system are given by partial pressure of H_2O (e), partial pressure of CO_2 (c) and temperature (T). First, we will describe the latent and sensible heat fluxes occurring between the canopy, ground, canopy airspace, and atmosphere. Then, we will elaborate on the coupled water vapor and CO_2 transport controlled by stomatal response to varying environmental conditions.

The two layer approach[13] used in this LSM splits the transport equations into canopy, ground, and atmospheric fluxes that are coupled via the canopy airspace (shown in Figure S11). In effect, there are four transport pathways: 1) sunlit canopy to canopy airspace, 2) shaded canopy to canopy airspace, 3) ground to canopy airspace, and 4) canopy airspace to atmosphere above canopy. The first three pathways must balance with the last pathway under the steady-state conditions. All transport equations use integrated flux-gradient relationships (also known as bulk transfer relations or an analogy to Ohm's law) to calculate fluxes as the difference in potentials between two points in space multiplied by a conductance (inverse of resistance). As previously mentioned, the index k in an equation represents either the sunlit or shaded big leaf; the forms of the equations are identical, but the states experienced by the each big leaf and its respective fluxes will differ.

S6.3.1 Latent and Sensible Heat Fluxes

The transport of water vapor from the canopy to the canopy air space (transpiration) consists of two steps: 1) transport from the leaf mesophyll cells through the stomatal opening ($LE_{l,k}$, Eqn. S37) and 2) transport through the laminar boundary layer at the leaf surface to the canopy air space (Eqn. S38). The transpiration through the stomata apertures is driven by potential differences in the stomatal cavity vapor pressure ($e_{i,k}$) and the vapor pressure at the surface of the leaf ($e_{s,j}$) and mediated by the stomatal aperture controlled by stomatal conductance $g_{s,k}$. Likewise, the transport from the leaf surface to the canopy air space is driven by the difference in $e_{s,j}$ and vapor pressure in the canopy air space (e_{ca}) and mediated by the laminar boundary layer conductance to water vapor (g_{bv}). Since we assume steady state and use Ohm's analogy to represent transport, we can treat these two pathways as two resistors in series and calculate the overall transpiration from the canopy in a single equation (Eqn. S39). Note that scaling from the individual leaf to the big leaf approximation is done simply by mulitplying by sunlit or shaded leaf area index (LAI_k). This assumes that all sunlit leaves have the same stomatal conductance and internal vapor pressure as do the shaded leaves. Additionally, we apply a mass-to-energy unit conversion (C_e) consisting of the latent heat of vaporization ($\mathscr{L}_v$), density of air (ρ_a), ratio of molar mass of water to molar mass of air (ε), and atmospheric pressure (P_{atm}). For simplicity, we have assumed a constant air density and have not modified it based on water vapor concentration or temperature. The LE equation is written assuming stomata on one side of the leaf as is common practice[13]. If a plant has stomata on both sides, it is usually accounted for in the stomatal conductance measurement and parameters.

$$LE_{l,k} = LAI_k \cdot C_e \cdot g_{s,k} \cdot \left(e_{i,k} - e_{s,k}\right) \tag{S37}$$

$$LE_{l,k} = LAI_k \cdot C_e \cdot g_{bv} \cdot \left(e_{s,k} - e_{ca}\right) \tag{S38}$$

$$LE_{l,k} = LAI_k \cdot C_e \cdot \frac{g_{s,k} \cdot g_{bv}}{g_{s,k} + g_{bv}} \cdot \left(e_{i,k} - e_{ca}\right) \tag{S39}$$

$$C_e = \frac{\mathscr{L}_v \cdot \rho_a \cdot \varepsilon}{P_{atm}} \tag{S40}$$

The description of sensible heat flux from the canopy is simpler than that of latent heat flux, as we assume no temperature gradient within a leaf. Therefore, heat transport is driven by temperature difference between the leaf ($T_{l,k}$) and canopy airspace (T_{ca}) only and mediated by the laminar boundary layer conductance to heat (g_{bh}). The result is scaled from a single leaf to the entire canopy by multiplying by the sunlit or shaded LAI as shown in Equation S41. The underlying assumption here is that all sunlit leaves have one temperature and all shaded leaves have another at each timestep. Furthermore, a conversion factor (C_h, Eqn. S41) consisting of ρ_a and specific heat at constant pressure (c_p) is required to make the transport in terms of enthalpy which is the conserved quantity (not temperature). The factor of 2 in Equation S41 represents transport from both sides of the leaf.

$$H_{l,k} = 2LAI_k \cdot C_h \cdot g_{bh} \cdot \left(T_{l,k} - T_{ca}\right) \tag{S41}$$

$$C_h = \rho_a \cdot c_p \tag{S42}$$

There are four unknown conductances that must be calculated. The stomatal conductance g_s will be covered in the next section as it is coupled to carbon assimilation. The laminar boundary layer conductances for water vapor and heat are assumed identical based on Reynold's analogy[13] and are calculated using equations derived from heat transfer experiments on rigid steel leaves (Eqn. S43). The calculation requires a turbulent transfer coefficient (C_l), a characteristic leaf dimension (d_l) and the friction velocity (u_*) measured at the flux tower.

$$g_{bv} = g_{bh} = \frac{C_l \cdot u_*}{d_l} \tag{S43}$$

Next, the transport of water and heat from the ground to the canopy airspace is shown in Equations S44-S45. Much like $LE_{l,k}$, latent heat flux from the ground (LE_g) consists of two conductances in series driven by the vapor pressure difference in ground (e_g) and canopy airspace (e_{ca}). The conductances represent vapor transport through the tortuous soil pores when soil is not saturated (g_{sv}) and the subsequent transport from the soil surface to the canopy airspace through a laminar boundary layer (g'_{av}). The sensible heat flux from the ground to canopy airspace H_g is driven by the difference in ground temperature T_g and T_{ca} mediated by conductance of heat between soil surface and canopy airspace (g'_{ah}).

$$LE_g = C_e \cdot \frac{g_{sv} \cdot g'_{av}}{g_{sv} + g'_{av}} \cdot (e_g - e_{ca}) \tag{S44}$$

$$H_g = C_h \cdot g'_{ah} \cdot (T_g - T_{ca}) \tag{S45}$$

The conductance for both heat and water vapor from the soil are again assumed equivalent by Reynold's analogy and is calculated using a turbulent transfer coefficient (C_g) and u_* as assumed in[16] (Eqn. S46). The turbulent transfer coefficient is balanced between bare soil and dense canopy values using Equations S47-S49. The reader is referred to[16] and references therein for justification of these parametrizations.

$$g'_{av} = g'_{ah} = C_g \cdot u_* \tag{S46}$$

$$C_g = W \cdot C_{g,bare} + (1-W) \cdot C_{g,dense} \tag{S47}$$

$$W = \exp(-LAI - SAI) \tag{S48}$$

$$C_{g,bare} = \frac{k}{0.13} \cdot \left(\frac{z_{om,g} \cdot u_*}{\nu} \right)^{-0.45} \tag{S49}$$

The additional conductance accounted for in unsaturated soils, g_{sv}, is calculated with Equation S50 using an estimate of the dry soil layer (DSL), the water vapor diffusivity (D_v) and a shape factor describing the tortuosity of the soil pores (τ). The value of g_{sv} approaches ∞ as the soil becomes saturated to an incipient level (θ_i) which was calibrated in our analysis. If g_{sv} is infinite, the conductance in Equation S44 simplifies to g'_{av}. The reader is again referred to[16] and references therein for justification of these parametrizations.

$$g_{sv} = \frac{D_v \cdot \tau}{DSL} \tag{S50}$$

$$D_v = 2.12 \times 10^{-5} \cdot \left(\frac{T_g + 273.15}{273.15}\right)^{1.75} \tag{S51}$$

$$DSL = D_{max} \cdot \frac{\theta_i - \theta_s}{\theta_i - \theta_{air}} \tag{S52}$$

$$\tau = \phi_{air}^2 \cdot \left(\frac{\theta_{sat} - \theta_{air}}{\theta_{sat}}\right)^{3/b} \tag{S53}$$

Lastly, the latent and sensible heat fluxes from the canopy airspace to the atmosphere at the measurement point z are described in Equations S54-S55. The potential differences are between vapor pressure and temperature in the canopy airspace (T_{ca} and e_{ca}) and the atmosphere at the flux tower measurement height (T_a and e_a). The conductance from the canopy airspace to the atmosphere is again the same for heat (g_{ah}) and vapor (g_{av}) by Reynold's analogy shown in Equation S56. The conductance is based on the Monin-Obukhov similarity theory (MOST)[23] also known as the 'log-law'. The momentum roughness length (z_{om}), heat/vapor roughness length (z_{oh}), and zero-plane displacement height (d_o) are empirical parameters. The z_{om} was determined from literature while the other two parameters are calculated using practical relationships[24] (Eqns. S57-S58). For this study, we neglected the impact of atmospheric stability on the atmospheric conductance term. These effects are usually handled by correction factors accounting for how density stratifications in the atmosphere enhance or suppress turbulent transport. However, the stability corrections add another level of complexity to the numerical scheme, as they are dependent on H and LE, and are not important to the overall question of this research.

$$LE = C_e \cdot g_{av} \cdot (e_{ca} - e_a) \tag{S54}$$

$$H = C_h \cdot g_{ah} \cdot (T_{ca} - T_a) \tag{S55}$$

$$g_{ah} = g_{av} = \frac{\overline{u} \cdot k^2}{\ln\left(\frac{z_m - d_o}{z_{om}}\right) \cdot \ln\left(\frac{z_m - d_o}{z_{oh}}\right)} \tag{S56}$$

$$z_{oh} = 0.1 z_{om} \tag{S57}$$

$$d_o = 0.7h \tag{S58}$$

In summary, Equations S37-S58 contain five prognostic variables: $T_{l,sl}$, $T_{l,sh}$, T_g, $g_{s,sl}$, and $g_{s,sh}$. An important assumption for scalar transport is that the vapor pressures $e_{i,k}$ and e_g are assumed to be dependent on $T_{l,k}$ and T_g via the Clausius-Clapeyron relationship[13]. Furthermore, the states of the canopy airspace, e_{ca} and T_{ca}, are completely determined by the states and conductances of the canopy, ground, and atmosphere. Substituting Equations S39, S41, S44, S45, S54 and S55 into Equations S10-S11 and solving for e_{ca} and T_{ca} yields weighted averages of the other conductances and states (Eqns. S59-S60). All other terms in the scalar transport equations are either forcing data, parameters, or constants. Therefore, we have at least five variables thus far that must be solved for.

$$e_{ca} = \frac{g_{av} \cdot e_a + g_{l,sl} \cdot e_{i,sl} + g_{l,sh} \cdot e_{i,sh} + g_{av,g} \cdot e_g}{g_{av} + g_{l,sl} + g_{l,sh} + g_{av,g}} \tag{S59}$$

$$T_{ca} = \frac{g_{ah} \cdot T_a + g_{bh} \cdot T_{l,sl} + g_{bh} \cdot T_{l,sh} + g_{ah,g} \cdot T_g}{g_{ah} + 2g_{bh} + g_{ah,g}} \tag{S60}$$

$$g_{l,k} = \frac{LAI_k \cdot g_{s,k} \cdot g_{bv}}{g_{s,k} + g_{bv}} \tag{S61}$$

S6.4 Stomatal Conductance and CO_2 Assimilation

Stomatal conductance is intrinsically tied to CO_2 assimilation as stomatal aperture and CO_2 gradient controls photosynthetic carbon fixation. We utilize a steady state, coupled stomatal conductance-photosynthesis scheme similar to[25] that balances CO_2 assimilation with CO_2 diffusion into the leaf. Specifically, we utilize the Medlyn stomatal conductance model[26] to represent stomatal conductance responses to atmospheric conditions coupled with the Farquhar, von Caemmerer, and Berry (1980) C3 photosynthesis model[27] (hereafter, referred to as FvCB model).

S6.4.1 Medlyn Stomatal Conductance Model

The Medlyn stomatal conductance model (Eqn. S62) is derived assuming plants optimize the ratio of carbon gain to water lost at each instant[26]. The solution of a resulting calculus of variations problem yields a relation where stomata close under higher vapor pressure deficit ($D_k = e_{i,k} - e_{s,k}$) and leaf surface CO_2 concentration (c_s), and open with higher CO_2 assimilation ($A_{n,k}$). This model provided a unifying framework for previously successful empirical methods[28]. The model is parametrized by the minimum stomatal conductance (g_o) and a species-specific slope parameter (g_1) related to the marginal carbon gain to water loss.

$$g_{s,k} = g_o + \left(1 + \frac{g_1}{\sqrt{D^k}}\right) \frac{1.6 A_{n,k}}{c_s / P_{atm}} \tag{S62}$$

The stomatal conductance model is coupled to the photosynthesis model via the term $A_{n,k}$ and the CO_2 diffusion equation (Eqn. S63). The transport of CO_2 into the leaf via diffusion is nearly identical to that of water vapor (Eqn. S39), with increases to stomatal and laminar boundary layer conductances of 1.6 and 1.4, respectively, to account for the differing diffusivities of CO_2 compared to H_2O.

$$A^d_{n,k} = \frac{g_{s,k} \cdot g_{bv}}{1.4 g_{s,k} + 1.6 g_{bv}} \cdot \frac{\left(c_{i,k} - c_{ca}\right)}{P_{atm}} \cdot 10^6 \tag{S63}$$

S6.4.2 FvCB C3 Photosynthesis Model

The FcVB model[27] represents the three limiting mechanisms of the Calvin Cycle for steady-state carbon assimilation from atmospheric CO_2: 1) the enzyme kinetics of Ribulose 1,5 bisphosphate carboxylase-oxyganese (Rubisco), 2) the rate of Ribulose 1,5 bisphosphate (RuBP) regeneration rate governed by ATP and NADPH created in the election transport chain of the light reactions, and 3) the amount of triose phosphates (starches) a plant can use. The equations here are for C3 photosynthesis only following[16].

Rubisco-limitation is represented using Michaelis-Menten (MM) kinetics that describe uptake velocity of a fixed amount of Rubisco when RuBP is saturated at an internal concentration of CO_2 (Eqn. S64). The equation determines the amount of CO_2 assimilated or released depending on whether Rubisco combines RuBP with CO_2 (carboxylation) or RuBP with O_2 (oxygenation). Thus, the equation requires values for partial pressure of oxygen in the leaf (o_i, Eqn. S65), MM constant for CO_2 (K_c, Eqn. S66), MM constant for O_2 (K_o, Eqn. S67), and the CO_2 compensation point (Γ, Eqn. S68).

$$A_{c,k} = V_{max25} \frac{c_{i,k} - \Gamma}{c_{i,k} + K_c\left(1 + o_i/K_o\right)} \tag{S64}$$

$$o_i = 0.209 \cdot P_{atm} \tag{S65}$$

$$K_c = 404.9 \times 10^{-6} \cdot P_{atm} \tag{S66}$$

$$K_o = 278.4 \times 10^{-3} \cdot P_{atm} \tag{S67}$$

$$\Gamma = 42.75 \times 10^{-6} \cdot P_{atm} \tag{S68}$$

The RuBP-limited assimilation rate (A_j, Eqn. S69), also known as the light-limited rate, describes conditions where the RuBP is limiting due to shortages in NADPH and ATP from the electron transport chain in the thykaloid of the mesophyll cells. A balance of the number of electrons required to create the required NADPH for RuBP regneration yields Equation S69 where the rate of electron transport (J) is a key quantity. The electron transport rate is itself co-limited between a maximum rate (J_{max25}) and the efficiency of photosystem II at delivering electrons (I_{PSII}, Eqn. S70) from the absorbed PAR by the leaf ($S_{l,k,par}$). The factor of 4.6 in Equation S70 represents unit conversion to quanta of energy[29]. The quantum efficiency of photosystem II (Φ_{PSII}) is usually taken to be 0.7[16].

$$A_{j,k} = J \frac{c_{i,k} - \Gamma}{4c_{i,k} + 8\Gamma} \tag{S69}$$

$$I_{PSII,k} = 0.5\Phi_{PSII}\left(4.6 \cdot S_{l,k,par}\right) \tag{S70}$$

$$\Theta_{PSII} \cdot J^2 - \left(I_{PSII,k} + J_{max25}\right) \cdot J + I_{PSII,k} \cdot J_{max25} = 0 \tag{S71}$$

The product-limited assimilation rate (A_p, Eqn. S72) represents the upper limit on assimilation based on the plant's need for the sugars. See[16] and sources within for justifications of the relationship with V_{max25}.

$$A_p = V_{max25}/6 \tag{S72}$$

Altogether, we want to calculate what the co-limitation of these three controls on the CO_2 assimilation of a plant. To do this, we use quadratic equations to estimate the co-limitation as laid out in[30] to allow a gradual transition across the three mechanisms and to account for additional limitations, rather than explicitly calculating any of the mechanisms separately. The Θ_{cj} and Θ_{ip} are empirical curvature factors that control for this gradual transition, given in[16]. The overall CO_2 assimilation A_k is given by the root of Equations S73 and S74. Lastly, we must remove from A_k the amount of CO_2 that is released through dark respiration R_d to get the overall net assimilation $A_{n,k}$ (Eqn. S75). $A_{n,k}$ is the amount of CO_2 assimilated from the atmosphere, balanced with leaf diffusion (Eqn. S60) for a big leaf as mediated by stomatal conductance.

$$\Theta_{cj} \cdot A_{i,k}^2 - (A_{c,k} + A_{j,k}) \cdot A_{i,k} + A_{c,k} \cdot A_{j,k} = 0 \tag{S73}$$

$$\Theta_{ip} \cdot A_k^2 - (A_{i,k} + A_{p,k}) \cdot A_k + A_{i,k} \cdot A_{p,k} = 0 \tag{S74}$$

$$A_{n,k} = A_k - R_d \tag{S75}$$

$$R_d = 0.015 \cdot V_{max25} \tag{S76}$$

For simplicity, we have omitted the temperature dependence of the photosynthetic parameters V_{max25}, J_{max25}, R_d, K_c, K_o, and Γ and simply use the values at 25^oC[31–33]. These dependencies are typically handled with an Arrhenius functions[13] to account for the breakdown or acceleration of various metabolic processes at high and low temperatures. Since the goal of this paper was to test the transpiration downregulation schemes, we omitted the temperature dependence due to the need for many more parameters to properly use the Arrhenius functions.

S6.4.3 Scale Correction of Photosynthetic Parameters

The maximum carboxylation rate of the Rubisco enzyme (V_{max25}) and the maximum electron transport rate (J_{max25}) are dependent on nitrogen availability in the leaf. Nitrogen has been been found to exponentially decay with relative cumulative leaf area in the canopy[34]; therefore, both V_{max25} and J_{max25} vary nonlinearly with plant height. For simplicity, we follow[20] for scaling V_{max25} and[22] for scaling J_{max25} to account for this nonlinear nitrogen profile. These methods differ form the optimality principles used in CLM v5[16].

The overall Rubisco carboxylation capacity of the canopy ($V_{l,max25}$) factoring in leaf nitrogen is give in Equation S77, where K_n is the extinction coefficient for leaf nitrogen content. The two big leaf model requires separate consideration of the sunlit and shaded big leaf[35] shown in Equations S77-S79. The maximum electron transport rate of the canopy ($J_{l,max25}$) factoring in leaf nitrogen is give in Equation S80, while the sunlit and shaded big leaf values are shown in Equations S81-S82. The values of $V_{l,k,max25}$ and $J_{l,k,max25}$ are used in place of the V_{max25} and J_{max25} parameters for the FvCB model described in the previous section.

$$V_{l,max25} = LAI \cdot V_{max25} \cdot [1 - \exp(-K_n)] \tag{S77}$$

$$V_{l,sl,max25} = LAI \cdot V_{max} \cdot \frac{1 - \exp(-K_n - K_b \cdot LAI)}{K_n + K_b \cdot LAI} \tag{S78}$$

$$V_{l,sh,max25} = V_{l,max25} - V_{l,sl,max25} \tag{S79}$$

$$J_{l,max25} = J_{max25} \cdot \frac{1 - \exp\left(-K'_d \cdot LAI\right)}{K'_d} \tag{S80}$$

$$J_{l,sl,max25} = J_{max25} \cdot \frac{1 - \exp\left(-[K'_d + K_b] \cdot LAI\right)}{K'_d + K_b} \tag{S81}$$

$$J_{l,sh,max25} = J_{l,max25} - J_{l,sl,max25} \tag{S82}$$

S6.5 Transpiration Downregulation

the transpiration downregulation schemes used in the paper are the empirical β and Plant Hydraulic Model schemes (PHM). We will discuss how each is implemented to suppress transpiration under soil water stress. The reader is referred to the main article for detailed discussion on the theoretical justification for the two methods.

S6.5.1 Well-Watered Transpiration

Before discussing the transpiration downregulation schemes, we must first clarify the terminology ‘well-watered’. As stated in the main article, well-watered refers to soil water conditions that do not cause any limitation to transpiration through stomatal closure via low leaf water potential. In other words, the transpiration meets the stomata-regulated atmospheric moisture demand—determined by the Medlyn model (Eqn. S62) and the vapor pressure deficit (D). This definition becomes slightly more ambiguous as we introduce a dual source, two big leaf model structure, as the states (vapor pressure and temperature) experienced by the hypothetical big leafs at a time step adjust to downregulation. Therefore, for clarity, the well-watered transpiration rate is the value corresponding to the states when there is no stomatal closure from soil moisture effects. Computationally, this is simple, since the well-watered rate is the LSM output when downregulation is turned off. This approach differs from CLM v5[16], which considers well-watered transpiration to be the rate under the downregulated states. This distinction between the two definitions of the well-watered rate will become important shortly, as the well-watered rate is a key variable in the transpiration downregulation schemes. Also, note that the well-watered rate is different between sunlit and shaded big leaf as they encounter differing temperatures, light, and vapor pressures.

S6.5.2 β Downregulation Schemes

As mentioned in the main article and in section S2, the LSM utilizes a Weibull function to represent the empirical β curve (Eqn. 16 in the main article). There are three variants of this method used: 1) a single β, 2) a 2-leaf β, and 3) a dynamic β. Since the method is empirical, there is not firm guidance on where within the plant to apply this downregulation, as some models apply it directly to well-watered stomatal conductance and other apply it to photosynthetic parameters like V_{max25}. Here, we apply β to the well-watered transpiration rate of the sunlit and shaded big leaf to maintain consistency with our minimalist analysis. The solution scheme section will discuss in greater detail how β is applied.

S6.5.3 PHM Downregulation Scheme

We will elaborate here on the PHM laid out in the main article and extend its formulation to the two-big leaf approach of the LSM. The PHM is similar to that in CLM v5[16,36], with simplification to soil-to-xylem, xylem-to-leaf, and leaf-to atmosphere segmentation. For readability the equations shown in the main article are repeated here. Each segment has a conductance curve that downregulates from the maximum conductance values based on water potentials through the segment. The conductivity equations follow closely the work of[4,37] and references therein. All parameter values and units for the following equations can be found in Table S7.

The soil-to-xylem conductance (g_{sx}, Eqn. S83) consists of the well-known unsaturated hydraulic conductivity curve for soil[9] and a maximum conductance value ($g_{sx,max}$, Eqn. S84). The downregulation function is parametrized by saturated soil water potential (ψ_{sat}), soil water retention exponent (b), unsaturated hydraulic conductivity exponent ($c = 2b + 3$), and a correction factor ($d = 4$) to account for roots' ability to reach water[38]. The $g_{sx,max}$ value is calculated using the saturated hydraulic conductivity ($k_{s,sat}$), specific weight of water ($\rho_w \cdot g$) and a length scale based on root area index (RAI), fine root diameter (d_r) and effective rooting depth (Z_r) to convert to conductance.

$$g_{sx}(\psi) = g_{sx,max} \cdot \left(\frac{\psi_{sat}}{\psi}\right)^{\frac{c-d}{b}} \tag{S83}$$

$$g_{sx,max} = \frac{k_{s,sat}}{\rho_w g}\sqrt{\frac{RAI}{d_R Z_r}} \cdot 10^{-6} \tag{S84}$$

The xylem-to-leaf conductance, g_{xl} (Eq. S85), is the maximum xylem-to-leaf conductance ($g_{xl,max}$, Eqn. S85) downregulated by a sigmoidal function[39] parametrized by the vulnerability exponent a and the xylem water potential (ψ_x) at 50% loss of conductance ($\psi_{x,50}$). The $g_{xl,max}$ is estimated using sapwood hydraulic conductivity (K_{sap}), and the height of vegetation (h_v).

$$g_{xl}(\psi) = g_{xl,max} \cdot \left[1 - \frac{1}{e^{a(\psi - \psi_{x,50})}}\right] \tag{S85}$$

$$g_{xl,max} = \frac{K_{sap}}{h_v \cdot \rho_w} \tag{S86}$$

The leaf-to-atmosphere conductance (Eq. S87) is the stomatal conductance for the sunlit and shaded leaf, $g_{s,k}$, downregulated from its well-watered value ($g_{s,ww,k}$) using a Weibull function parametrized by a shape factor (b_l) describing stomatal sensitivity and the leaf water potential at 50% loss of conductance ($\psi_{l,50}$)[8]. The $g_{s,ww,k}$ value is calculated using the Medlyn model previously discussed in Equation S59[26]. The values for stomatal conductance are defined for both sunlit and shaded leaf by index k as they will almost always differ.

$$g_{s,k} = g_{s,ww,k} \cdot e^{-\left(\frac{\psi_{l,k}}{\psi_{l,50}}\right)^{b_l}} \tag{S87}$$

In order to calculate the water flux through each segment, we must utilize a Kirchhoff transform (Eqn. S88) to account for the the varying potential (and conductance) along each segment[40]. The transform is only performed on the soil-to-xylem and xylem-to-leaf segments as the distance traveled through the leaf to stomata is assumed negligible. The total flux potential for soil-to-xylem ($\Phi_{sx}(\psi)$, Eqn. S89) and xylem-to-leaf ($\Phi_{xl}(\psi)$, Eqn. S90) give an upper limit on the water that could be extracted from a segment based on the potential. Using this linearized flow theory, the flux through each segment is simply calculated by taking the difference in total flux potential between the end points of each segment.

$$\Phi(\psi) = \int_{-\infty}^{\psi} K\left(\psi'\right) d\psi' \tag{S88}$$

$$\Phi_{sx}(\psi) = \frac{b \cdot g_{sx,max} \cdot \psi}{b - c + d} \cdot \left(\frac{\psi_{sat}}{\psi}\right)^{\frac{c-d}{b}} \tag{S89}$$

$$\Phi_{xl}(\psi) = g_{xl,max} \cdot \left[\frac{\ln\left(e^{-a\psi} + e^{-a\psi_{50}}\right)}{a} + \psi\right] \tag{S90}$$

The two-big leaf configuration of this model requires five total segments: soil-to-xylem, xylem-to-sunlit leaf, xylem-to-shaded leaf, sunlit leaf-to-atmosphere, and shaded leaf-to-atmosphere. The underlying assumption is that the transport from xylem to the sunlit and shaded leaf is completely independent. The transport in each segment is shown below in Equations S91-S93. Note these equations are the same as Equations 15-17 in the main article except adapted for the two big leaf configuration.

$$LE_{sx} = [\Phi_{sx}(\psi_s) - \Phi_{sx}(\psi_x)] \cdot \rho_w \cdot \mathscr{L}_v \tag{S91}$$

$$LE_{xl,k} = \left[\Phi_{xl}(\psi_x) - \Phi_{xl}(\psi_{l,k})\right] \cdot \rho_w \cdot \mathscr{L}_v \tag{S92}$$

$$LE_{la,k} = LAI_k \cdot g_{s,k} \cdot \left(e_{i,k} - e_{s,k}\right) \cdot C_e \tag{S93}$$

We assume a steady-state solution where the supply through the soil-plant system equals the atmospheric moisture demand. This problem can be solved using a Newton-Raphson method as done in CLM v5[16]. However, this method was found to be unstable under certain conditions; therefore, we opted to use nonlinear least squares in MATLAB (*lsqnonlin*) to solve the problem. We used the trust-region-reflective method which is a quasi-Newton method that handles bounded constraints on the decision variable. The optimization problem is laid out in Equations S94-S96. The decision variables (ψ, Eqn. S96) are xylem, sunlit leaf, and shaded leaf water potentials that balances the flow through all segments while the residuals (R, Eqn. S95) ensure this balance with values of 0. The constraints in the optimization problem keep the water potentials between $\psi_{s,sat}$ and a value of -30 MPa.

$$\psi^* = \min_{\psi} \quad \|R\|^2 \qquad \text{s.t.} \quad \psi \in (-30,\, \psi_{s,sat}) \tag{S94}$$

$$R = \begin{bmatrix} LE_{sx} - \sum_{k=1}^{2} LE_{xl,k} \\ LE_{xl,sl} - LE_{la,sl} \\ LE_{xl,sh} - LE_{la,sh} \end{bmatrix} \tag{S95}$$

$$\psi = \begin{bmatrix} \psi_{l,sl} \\ \psi_{l,sh} \\ \psi_x \end{bmatrix} \tag{S96}$$

S6.6 LSM Solution Scheme

There are numerous ways to solve the steady-state dual source scheme depending on how the equations and unknowns have been defined. Here, we have created our own method, similar to CLM v5. There are two overall computational schemes or solvers: a well-watered solver and a transpiration downregulation solver. In the well-watered scheme, there are two levels of computation: the surface energy budget solver (outer solver) and the scalar transport solver (inner solver). For the transpiration downregulation scheme, well-watered solutions are adjusted in a separate solver based on soil moisture availability. Our solvers use optimization routines rather than the linearized, Newton-Raphson methods used in CLM v5 for several reasons: 1) numerical derivatives are required for both methods, 2) the optimization routine guards against solution divergence, 3) the optimization routine is simple to set up, and 4) speed between the two methods at our scale is essentially the same.

S6.6.1 Well-Watered Solver

The well-watered solver is the primary solution scheme of the LSM, which is run for every simulation with and without transpiration downregulation. The solver consists of two nested least squares optimization problems, which have been referred to as the outer and inner solvers for simplicity. There are six overall state variables that must be adjusted to balance the surface energy budget (Eqn. S5) for this steady-state problem: $T_{l,k}$, T_g, $c_{i,k}$ and e_{ca}. The outer solver is concerned with balancing the surface energy budget by finding the correct leaf ($T_{l,k}$) and ground (T_g) temperatures, whereas the inner solver is focused on finding the correct internal leaf carbon concentrations ($c_{i,k}$) and canopy water vapor pressure (e_{ca}) that balance the LE and H leaving the ground and canopy with the transport from the canopy airspace to atmosphere.

The outer solver is a three dimensional nonlinear least squares problem shown in Equations S97-S99. The residuals being minimized (R^o) are the sunlit big leaf, shaded big leaf, and ground energy balances in Equations S6-S8, while the decision variables (T) are the temperatures of these three respective compartments. The outer solver is illustrated in (Fig. S12) as it begins by gathering all the environmental forcing data for a particular time step (section S4). The outer solver then initiates a guess for the three temperatures based on the air temperature. The next step is to solve the GvL radiative transfer model to obtain the net radiation R_n for the three compartments and their breakdown into PAR, NIR, and longwave components. At this point, the temperatures are sent to the inner solver to determine the scalar fluxes from the ground, canopy, and canopy airspace under these fixed temperatures and states. Once the inner solver finds the $c_{i,k}$ and e_{ca} that balances Equations S10-S11, the scalar fluxes for all compartments are calculated. The outer solver then checks to see if the net radiation in each compartment equals the scalar fluxes. If not, the temperatures are adjusted based on the optimization routine and the process is repeated until convergence.

$$
\begin{aligned}
T^* = \min_{T} \quad & \|R^o\|^2 \\
\text{s.t.} \quad & T \in (0, 40)
\end{aligned}
\tag{S97}
$$

$$
R^o = \begin{bmatrix} S_{l,sl,par} + S_{l,sl,nir} + L_{l,sl} - H_{l,sl} - LE_{l,sl} \\ S_{l,sh,par} + S_{l,sh,nir} + L_{l,sh} - H_{l,sh} - LE_{l,sh} \\ S_{g,par} + S_{g,nir} + L_g - H_g - LE_g - G_g \end{bmatrix}
\tag{S98}
$$

$$
T = \begin{bmatrix} T_{l,sl} \\ T_{l,sh} \\ T_g \end{bmatrix}
\tag{S99}
$$

The inner solver is also a three dimensional nonlinear least squares problem within the outer solver shown in Equations S100-S102. The inner solver is given temperatures and states of the two big leaves, ground, and air and must find the internal CO_2 concentrations that balance plant carbon synthesis with leaf diffusion, as well as the canopy water vapor pressure that balances transport from ground and plants with that to the atmosphere. The inner solver is shown in Figure S12 as the light gray indented panels. First, values of $c_{i,k}$ and e_{ca} are guessed based on atmospheric conditions. Then the FvCB model is solved to calculate the net CO_2 assimilation of each leaf ($A_{n,k}$), which must be matched by the Medlyn stomatal conductance model and leaf diffusion. A neat trick introduced in CLM v5[16] is to substitute the diffusion equation into the Medlyn equation to obtain a quadratic equation whose larger root is the solution for $g_{s,k}$ (Eqns. S103-S105). Using $g_{s,k}$, the internal carbon concentration from leaf diffusion ($c^{+}_{i,k}$) is calculated and checked against the assumed value of the solver $c_{i,k}$. Once $g_{s,k}$ has been determined, we can use Equation S59 to calculate a check on the canopy airspace water vapor pressure (e^{+}_{ca}). These values are adjusted by the optimization routine until convergence criteria is met. The results are then sent back out to the outer solver.

$$x^* = \min_{x} \quad \|R^i\|^2 \qquad \text{s.t.} \quad x \in (0, 40) \tag{S100}$$

$$R^i = \begin{bmatrix} c^{+}_{i,sl} - c_{i,sl} \\ c^{+}_{i,sh} - c_{i,sh} \\ e^{+}_{ca} - e_{ca} \end{bmatrix} \tag{S101}$$

$$x = \begin{bmatrix} c_{i,sl} \\ c_{i,sh} \\ e_{ca} \end{bmatrix} \tag{S102}$$

$$g_{s,j}^2 - \left[2 \cdot g_o + 2 \cdot C_{1,j} + \frac{C_{1,j}^2 \cdot g_1^2}{g_{bv} \cdot C_{2,j}} \right] g_{s,j} + \left[g_o^2 + 2 \cdot C_{1,j} \cdot g_o + C_{1,j}^2 \left(1 - \frac{g_1^2}{C_{2,j}} \right) \right] = 0 \tag{S103}$$

$$C_{1,j} = \frac{1.6 \cdot A_{n,j} \cdot P_{atm}}{c_{s,j} \cdot 10^6} \tag{S104}$$

$$C_{2,j} = \frac{e_{i,j} - e_{ca}}{1000} \tag{S105}$$

S6.6.2 Transpiration Downregulation Solver

The transpiration downregulation solver is an additional solver used after the well-watered solver to account for the effect of soil water stress on stomatal conductance and, in turn, on the scalar fluxes and plant microclimate. The solver scheme is a single least squares problem (Eqn. S106) in five dimensions of leaf temperatures and conductances as well as ground temperature (Eqn. S108). As in the well-watered solver, the first three residuals are the surface energy balance for the big leaves and ground (Eqn. S107). The final two residuals (Eqn. S109) ensure that the transpriation from the canopy calculated by the scalar transport module match the value calculated by the selected downregulation method; either β or PHM. For the β method, the downregulated transpiration is simply β multiplied by the well-watered transpriation rate $LE_{l,k,ww}$. For the the PHM method, the downregulated transpiration rate ($LE_{l,k,phm}$) is the solution to the PHM that balances supply and demand (Eqns. S94-S96).

The solver scheme is laid out in Figure S13 where it initializes the five decision variables from the well-watered solution. For the set temperatures and conductances we are able to re-calculate the longwave radiation, carbon assimilation, scalar fluxes and states. At this point, we can calculate the the surface energy budget residuals in Equation S107. Now there is a choice to make whether to select the β model or the PHM. The β model is less computationally expensive as we simply multiply β by the already calculated $LE_{l,k,ww}$. Any of the three β methods (β_s, β_{2L}, and β_{dyn}) can be applied at this point as there is no real computational difference between the three, just different β values are multiplied by the well-watered rates. The PHM scheme is slightly more complex as we must solve the three-dimensional least squares problem to balance supply and demand. However, both schemes then check the last two residuals (Eqn. S109) to ensure the transpiration from the scalar transport module (Eqn. S39) match the downregulation scheme transpiration. If the residual does not converge the solver adjusts the decision variable and repeats.

This transpiration downregulation scheme is different than that proposed by CLM v5[16] not only numerically but also in how the well-watered transpiration is defined. As seen in our scheme (Fig. S13), our well-watered transpiration is fixed during the scheme. We opted for this because the states of the plant microclimate under well-watered conditions are different then under downregulation. Therefore, under the same atmospheric forcings our method is consistent with what we would expect to see if the soil was saturated compared to when it is dry. The method in CLM v5 continually updates the well-watered transpiration during the downregulation solver. Essentially, as the microclimate states change during downregulation, CLM v5 re-calculates the well-watered stomatal conductance according to the Medlyn model and uses that in the downregulation schemes. This creates a positive feedback that increases transpiration suppression compared to our method. Also, the well-watered transpiration rate calculated in this method is the value that would be experienced in a certain plant microclimate and not necessarily under the atmospheric forcings. It is difficult to determine which method is most realistic, but they give very different values for downregulation. We think our definition of well-watered transpiration is more appropirate to defining the stomata-regulated atmospheric moisture demand so that is what was used in this analysis.

$$x^* = \min_x \quad \|R^t\|^2 \qquad \text{s.t.} \quad x \in (0, 40) \tag{S106}$$

$$R^t = \begin{bmatrix} S_{l,sl,par} + S_{l,sl,nir} + L_{l,sl} - H_{l,sl} - LE_{l,sl} \\ S_{l,sh,par} + S_{l,sh,nir} + L_{l,sh} - H_{l,sh} - LE_{l,sh} \\ S_{g,par} + S_{g,nir} + L_g - H_g - LE_g - G_g \\ R^t_{(4)} \\ R^t_{(5)} \end{bmatrix} \tag{S107}$$

$$x = \begin{bmatrix} T_{l,sl} \\ T_{l,sh} \\ T_g \\ g_{l,sl} \\ g_{l,sh} \end{bmatrix} \tag{S108}$$

$$R^t_{(4,5)} = \begin{cases} LE_{l,k,phm} - LE_{l,sl} & \text{if PHM scheme} \\ LE_{l,k} - \beta \cdot LE_{l,k,ww} & \text{if } \beta \text{ scheme} \end{cases} \tag{S109}$$

Surface Energy Budget

$R_n = S_{in} - S_{out} + L_{in} - L_{out} = H + LE + G$

Radiation Model: Goudriaan and Van Laar (1994)

Photosynthesis Model: Farquhar (1980)

Plant Hydraulics Model: Similar to Manzoni (2013)

Model Structure: Dual source, 2-Big Leaf Approximation

Model Forced With

- Vapor Pressure Defecit
- Air Temperature
- Soil Moisture
- Ground Heat Flux
- Streamwise Velocity
- Incoming Shortwave Radiation
- Incoming Longwave Radiation
- CO_2 Concentration
- Air Pressure

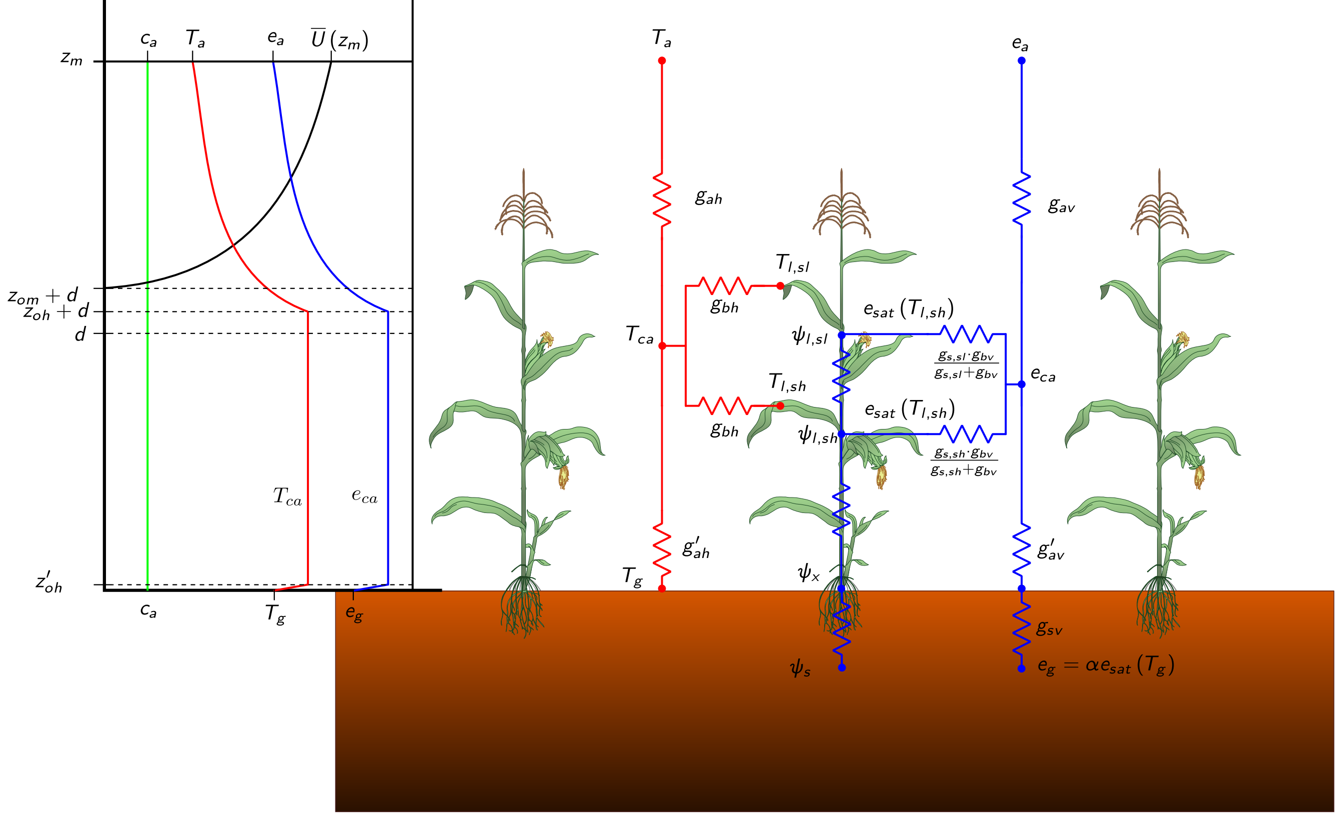

Figure S11. Schematic of our two big leaf, dual-source land surface model. The potentials and resistors indicate the scalar transport between the sunlit and shaded big leaf approximations, ground, canopy airspace and atmosphere. To the left are the assumed profiles of water vapor pressure deficit e, temperature (T), CO_2 partial pressure (c), and streamwise mean velocity ($\overline{U}$). The main modules used are laid out in text as well as the environmental forcings used from the US-Me2 Ameriflux site for our simulations.

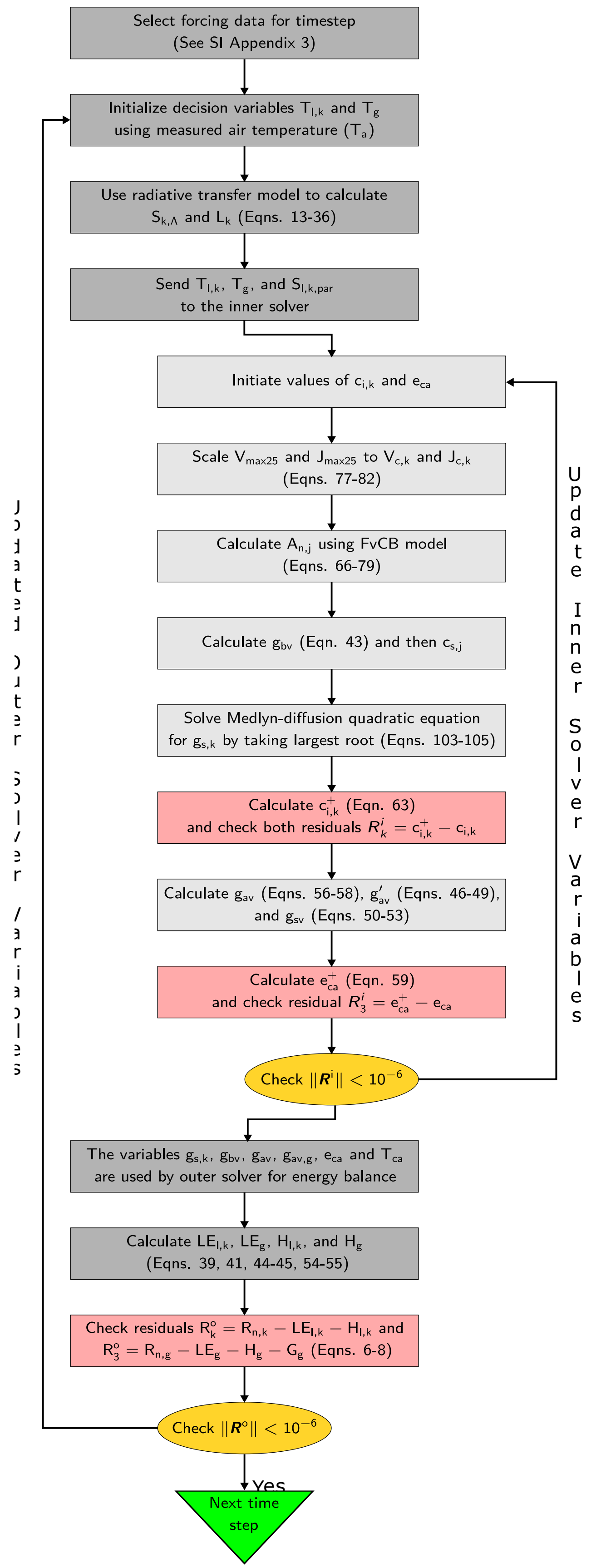

Figure S12. The well-watered solver solution scheme representing the outer solver (dark gray) and inner solver (light gray). Light red panels indicate a step where a residual to the nonlinear least squares problem is calculated and yellow indicates checking values of the residuals.

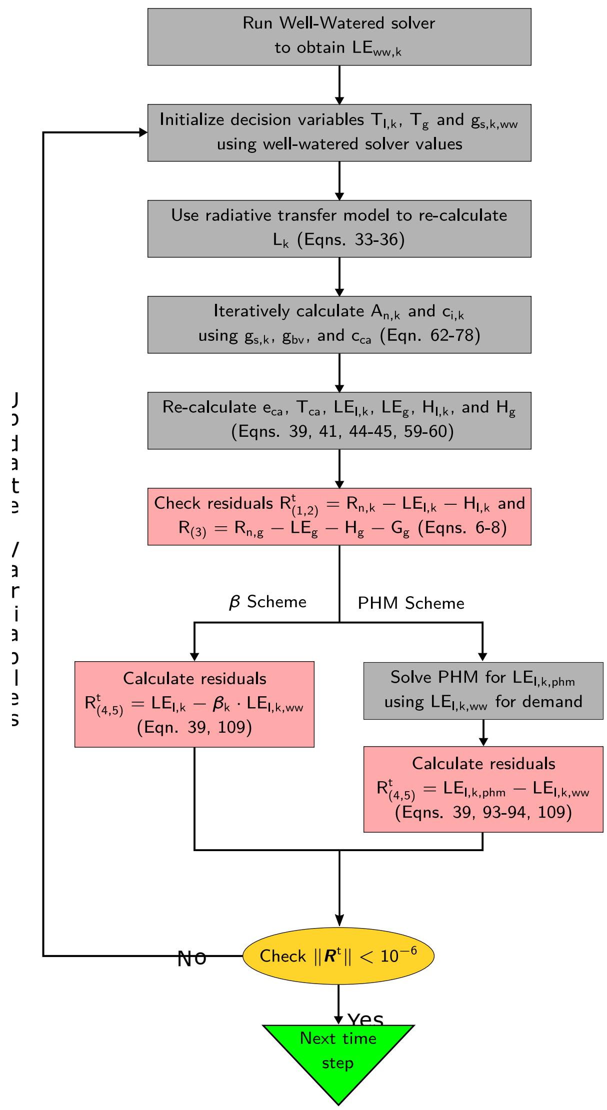

Figure S13. The transpiration downregulation scheme that is used after the well-watered solver to re-caclulate fluxes and states as plants reduce transpiration from soil water stress. Light red panels indicate a step where a residual to the nonlinear least squares problem is calculated and yellow indicates checking values of the residuals. There are two separate choices for downregulation: the β model and the Plant Hydraulic Model (PHM). See text for more details.

S7 LSM Variables, Parameters, and Forcings

The sheer volume of equations and data discussed in this supplemental materials make it necessary to provide a comprehensive table of variables, parameters, and constants with sources where necessary. This table has been split up based on the sections describing the LSM: radiative transfer (Table S4), scalar transport (Table S5), coupled stomatal conductance and photosynthesis (Table S6), transpiration downregulation (Table S7), and constants (Table S8). For each table, except the constants, the table is broken down into subscripts, fluxes and states, forcing data, and parameters. The 'subscripts' section is used to cut down on table entries as many subscripts are used on fluxes and parameters to describe their position in the the dual source, two big leaf framework; the variable names are shown in the specific sections. The 'fluxes and states' section shows the main fluxes and states used in the section without all the positional subscripts. The 'forcing data' section highlights the US-Me2 site data used to force the model discussed in section S4. The 'parameters' section contains all the functional and constant parameters used along with values and sources if constant.

Table S4. The main fluxes, states and parameters used by the radiative transfer module of the LSM.

Name	Description	Value	Units	Sources
Subscript				
l	Plant canopy	-		
sl	Sunlit big leaf	-		
sh	Shaded big leaf	-		
k	Sunlit or shaded big leaf	-		
par	Photosynthetically active radiation (PAR)	-		
nir	Near infrared radiation (NIR)	-		
Λ	PAR or NIR	-		
b	Direct beam radiation	-		
d	Diffuse radiation	-		
sb	Scattered beam radiation	-		
in	Incoming radiation	-		
out	Outgoing radiation	-		
Fluxes and States				
S	Absorbed shortwave radiation	-	$W{\cdot}m^{-2}$	
L	Absorbed longwave radiation	-	$W{\cdot}m^{-2}$	
T	Temperature	-	^{o}C	
Forcing Data				[41]
S_{in}	Incoming shortwave radiation	-	$W{\cdot}m^{-2}$	
$S_{in,par}$	Incoming PAR	-	$W{\cdot}m^{-2}$	
$S_{in,par,d}$	Diffuse incoming PAR	-	$W{\cdot}m^{-2}$	
L_{in}	Incoming longwave radiation	-	$W{\cdot}m^{-2}$	
T_a	Air temperature at measurement height	-	^{o}C	
Parameters				
K	Extinction coefficient	-	-	
K'	Extinction coefficient corrected for single-scattering	-	-	
$\alpha_{l,par}$	PAR leaf absorption coefficient	0.74	-	Calibrated
$\alpha_{l,nir}$	NIR leaf absorption coefficient	0.43	-	Calibrated
LAI	Leaf area index	3.2	m^2 leaf area$\cdot m^{-2}$ ground area	Calibrated
τ	Transmissivity	-	-	
$G(Z)$	Mean leaf angle	-	radians	
Z	Solar zenith angle	-	radians	
χ_l	Leaf angle distribution parameter	0.11	-	Calibrated
$\rho_{l,h}$	Leaf reflectance for infinite horizontal canopy	-	-	
ρ_l	Plant canopy reflectance for infinite canopy	-	-	
ρ_l'	Plant canopy reflectance accounting for ground reflectance	-	-	
$\rho_{g,par}$	PAR ground reflectance	0.1	-	[29]
$\rho_{g,nir}$	NIR ground reflectance	0.2	-	[29]
δ_l	Fraction of longwave radiation absorbed by canopy	-	-	
F_k	Fraction of sunlit or shaded leaf area index	-	-	

Table S5. The main fluxes, states and parameters used by the scalar transport module of the LSM.

Name	Description	Value	Units	Sources
Subscript				
l	Plant canopy	-		
sl	Sunlit big leaf	-		
sh	Shaded big leaf	-		
k	Sunlit or shaded big leaf	-		
i	Inside the stomatal cavity of the leaf	-		
s	On the leaf surface	-		
g	Ground/soil	-		
ca	Canopy airspace	-		
a	Atmosphere above canopy at measurement height	-		
Fluxes and States				
LE	Latent heat flux	-	$W \cdot m^{-2}$	
H	Sensible heat flux	-	$W \cdot m^{-2}$	
e	Water vapor pressure	-	Pa	
T	Temperature	-	^{o}C	
c	CO_2 partial pressure	-	Pa	
Forcing Data				41
$\overline{u}$	Mean streamwise velocity	-	$m \cdot s^{-1}$	
u^{*}	Friction velocity	-	$m \cdot s^{-1}$	
θ_s	Soil water content at 50 cm depth	-	m^3 water$\cdot m^{-3}$ soil	
e_a	Water vapor pressure at measurement height	-	Pa	
T_a	Water vapor pressure at measurement height	-	^{o}C	
G	Ground heat flux	-	$W \cdot m^{-2}$	
Parameters				
g_s	Stomatal conductance	-	mol $H_2O \cdot m^{-2} \cdot s^{-1}$ or $m \cdot s^{-1}$	
g_{bv} or g_{bh}	Leaf laminar boundary layer water vapor/heat conductance	-	$m \cdot s^{-1}$	
g_{av} or g_{ah}	Atmospheric water vapor/heat conductance	-	$m \cdot s^{-1}$	
g_{sv}	Soil pore to soil surface water vapor conductance	-	$m \cdot s^{-1}$	
g'_{av} or g'_{ah}	Soil to canopy airspace water vapor/heat conductance	-	$m \cdot s^{-1}$	
LAI	Leaf area index	3.2	m^2 leaf area$\cdot m^{-2}$ ground area	Calibrated
SAI	Stem area index	0.5	m^2 stem area$\cdot m^{-2}$ ground area	10
C_l	Leaf turbulent transfer coefficient	0.01	$m \cdot s^{-1}$	16
d_l	Characteristic leaf dimension	0.04	m	16
C_g	Ground turbulent transfer coefficient	-	$m \cdot s^{-1}$	
$C_{g,bare}$	Bare ground turbulent transfer coefficient	-	$m \cdot s^{-1}$	
$C_{g,dense}$	Dense canopy ground turbulent transfer coefficient	0.004	$m \cdot s^{-1}$	16
z_{om}	Atmospheric momentum roughness length	1	m	24
d_o	Zero-plane displacement	-	m	
z_{ov} or z_{ov}	Atmospheric water vapor/heat roughness length	0.1	m	24
$z_{om,g}$	Ground momentum roughness length	0.01	m	16
D_v	Water vapor diffusivity	-	$m^2 \cdot s^{-1}$	
DSL	Depth of dry soil layer	-	m	
D_{max}	Maximum dry layer thickness	0.015	m	
θ_{sat}	Saturated soil water content (porosity)	0.57	m^3 water$\cdot m^{-3}$ soil	42
θ_i	Soil water content where g_{sv} begins	0.57	m^3 water$\cdot m^{-3}$ soil	Calibrated
θ_{air}	Volumetric air content in soil pores	-	m^3 air$\cdot m^{-3}$ soil	
ϕ_{air}	Air filled pore space	-	m^3 air$\cdot m^{-3}$ pres	
τ	Soil pore tortuosity	-	-	
b	Brooks-Corey soil retention curve exponent	5.05	-	Calibrated
z	Measurement height	32	m	41
h_v	Vegetation height	18	m	41

Table S6. The main fluxes, states and parameters used by the coupled stomatal conductance-photosynthesis module of the LSM.

Name	Description	Value	Units	Sources
Subscript				
l	Plant canopy	-		
sl	Sunlit big leaf	-		
sh	Shaded big leaf	-		
k	Sunlit or shaded big leaf	-		
i	Inside the stomatal cavity of the leaf	-		
s	On the leaf surface	-		
g	Ground/soil	-		
ca	Canopy airspace	-		
Fluxes and States				
A_n	Net CO_2 assimilation rate	-	mol $CO_2 \cdot m^{-2} \cdot s^{-1}$	
A_c	Rubisco-limited CO_2 assimilation rate	-	mol $CO_2 \cdot m^{-2} \cdot s^{-1}$	
A_j	Light-limited CO_2 assimilation rate	-	mol $CO_2 \cdot m^{-2} \cdot s^{-1}$	
A_p	Product-limited CO_2 assimilation rate	-	mol $CO_2 \cdot m^{-2} \cdot s^{-1}$	
A	CO_2 assimilation rate	-	mol $CO_2 \cdot m^{-2} \cdot s^{-1}$	
c	CO_2 partial pressure		Pa	
Forcing Data				41
P_{atm}	Atmospheric Pressure	-	Pa	
Parameters				
g_s	Stomatal conductance	-	mol $H_2O \cdot m^{-2} \cdot s^{-1}$ or $m \cdot s^{-1}$	
g_1	Medlyn slope parameter	0.88	$kPa^{0.5}$	Calibrated
g_o	Minimal stomatal conductance	10e-4	mol $H_2O \cdot m^{-2} \cdot s^{-1}$ or $m \cdot s^{-1}$	16
g_{bv}	Leaf laminar boundary layer water vapor	-	$m \cdot s^{-1}$	
V_{max25}	Max Rubisco assimilation rate at 25^{o}C	122	mol $CO_2 \cdot m^{-2} \cdot s^{-1}$	Calibrated
J_{max25}	Max assimilation rate based on electron transport at 25^{o}C	256	mol photons$\cdot m^{-2} \cdot s^{-1}$	$2.1 \cdot V_{max25}$
Γ	CO_2 compensation point	-	mol $CO_2 \cdot m^{-2} \cdot s^{-1}$	
o_i	O_2 partial pressure	-	Pa	
K_c	Rubisco Michaelis-Menten rate constant for carboxylation	-	Pa	
K_o	Rubisco Michaelis-Menten rate constant for oxidation	-	Pa	
K_n	Nitrogen extinction coefficient	0.7	-	16
I_{PSII}	Efficiency of photosystem II to deliver electrons	-	mol photons $\cdot m^{-2} \cdot s^{-1}$	
Φ_{PSII}	Quantum efficiency of photosystem II	0.7	-	16
Θ_{PSII}	Curvature factor J_{max25} and I_{PSII} co-limitation	0.85	-	16
Θ_{cj}	Curvature factor A_c and A_j co-limitation	0.98	-	16
A_i	CO_2 assimilation rate co-limited by A_c and A_j	-	mol $CO_2 \cdot m^{-2} \cdot s^{-1}$	
Θ_{ip}	Curvature factor A_i and A_p co-limitation	0.95	-	16
R_d	Dark respiration rate		mol $CO_2 \cdot m^{-2} \cdot s^{-1}$	

Table S7. The main fluxes, states and parameters used by the transpiration downregulation module of the LSM.

Name	Description	Value	Units	Sources
Subscript				
l	Plant canopy	-		
sl	Sunlit big leaf	-		
sh	Shaded big leaf	-		
k	Sunlit or shaded big leaf	-		
i	Inside the stomatal cavity of the leaf	-		
s	On the leaf surface	-		
g	Ground/soil	-		
ca	Canopy airspace	-		
sx	Soil-to-xylem	-		
xl	Xylem-to-leaf	-		
la	Leaf-to-atmosphere	-		
ww	Well-watered rate	-		
max	Maximum value	-		
Fluxes and States				
LE	Latent heat flux	-	mol CO_2·m^{-2}·s^{-1}	
ψ	Water potential	-	MPa	
e	Water vapor pressure	-	Pa	
Forcing Data				[41]
θ_s	Soil water content at 50 cm depth	-	m^3 water·m^{-3} soil	
Parameters				
g_s	Stomatal conductance	-	mol H_2O·m^{-2}·s^{-1} or m·s^{-1}	
g	Segment-specific conductance	-	m·s^{-1}·MPa^{-1}	
$\psi_{s,sat}$	Saturated soil water potential	-1e-3	MPa	Calibrated
b	Brooks-Corey soil retention curve exponent	5.05	-	Calibrated
c	Brooks-Corey hydraulic conductivity exponent	-	-	
d	Adjusting factor for roots in soil conductance	4	-	[37]
$K_{s,sat}$	Saturated soil hydraulic conductivity	10	m·d^{-1}	Calibrated
RAI	Root area index	11	m^2 root area·m^{-2} ground area	[11]
d_r	Fine root diameter	5e-04	m	[11]
Z_r	Effective rooting depth	0.1	m	[42]
$\psi_{x,50}$	Xylem water potential at 50% loss of conductance	-9.9	MPa	Calibrated
a	Xylem vulnerability curve shape parameter	0.3	-	Calibrated
K_{sap}	Sapwood hydraulic conductivity	9.30E-04	kg·m^{-1}·s^{-1}·MPa^{-1}	Calibrated
h_v	Vegetation height	18	m	[41]
$\psi_{l,50}$	Leaf water potential at 50% loss of conductance	-9.9	MPa	Calibrated
b_l	Leaf vulnerability curve shape parameter	0.3	-	Calibrated
LAI	Leaf area index	3.2	m^2 leaf area·m^{-2} ground area	Calibrated
Φ	Flux potential from Kirchhoff transform	-	kg·s^{-1}	

Table S8. The main physical constants used in the LSM.

Name	Description	Value	Units
ρ_w	Density of water	1000	$kg{\cdot}m^{-3}$
ρ_a	Density of air	1.2	$kg{\cdot}m^{-3}$
ε	Molar ratio of water to air	0.622	-
$\mathscr{L}_v$	Latent heat of vaporization	2.50E+06	$J{\cdot}kg^{-1}$
k	von Karmen constant	0.4	-
ν	Kinematic viscosity	1.50E-05	$m^2{\cdot}s^{-1}$
R_g	Universal gas constant	8314	$J{\cdot}K^{-1}{\cdot}mol^{-1}$
c_p	Specific heat of air at constant pressure	1004	$J{\cdot}kg^{-1}{\cdot}K^{-1}$

References

1. Foken, T. The energy balance closure problem: An overview. *Ecol. Appl.* **18**, 1351–1367, DOI: 10.1890/06-0922.1 (2008).

2. Razavi, S. & Gupta, H. V. A new framework for comprehensive, robust, and efficient global sensitivity analysis: 2. Application. *Water Resour. Res.* **52**, 440–455, DOI: 10.1002/2015WR017559 (2016).

3. Razavi, S., Sheikholeslami, R., Gupta, H. V. & Haghnegahdar, A. VARS-TOOL: A toolbox for comprehensive, efficient, and robust sensitivity and uncertainty analysis. *Environ. Model. Softw.* **112**, 95–107, DOI: 10.1016/j.envsoft.2018.10.005 (2019).

4. Manzoni, S., Vico, G., Katul, G., Palmroth, S. & Porporato, A. Optimal plant water-use strategies under stochastic rainfall. *Water Resour. Res.* **50**, 1–16, DOI: 10.1002/2014WR015375 (2014).

5. Couvreur, V. *et al.* Water transport through tall trees: A vertically explicit, analytical model of xylem hydraulic conductance in stems. *Plant, Cell & Environ.* **41**, 1821–1839, DOI: 10.1111/pce.13322 (2018).

6. Manzoni, S. *et al.* Optimizing stomatal conductance for maximum carbon gain under water stress: a meta-analysis across plant functional types and climates. *Funct. Ecol.* **25**, 456–467, DOI: 10.1111/j.1365-2435.2010.01822.x (2011).

7. Choat, B. *et al.* Global convergence in the vulnerability of forests to drought. *Nature* **491**, 752–755, DOI: 10.1038/nature11688 (2012).

8. Klein, T. The variability of stomatal sensitivity to leaf water potential across tree species indicates a continuum between isohydric and anisohydric behaviours. *Funct. Ecol.* **28**, 1313–1320, DOI: 10.1111/1365-2435.12289 (2014).

9. Clapp, R. B. & Hornberger, G. M. Empirical equations for some soil hydraulic properties. *Water Resour. Res.* **14**, 601–604, DOI: 10.1029/WR014i004p00601 (1978).

10. Kattge, J. *et al.* TRY plant trait database – enhanced coverage and open access. *Glob. Chang. Biol.* **26**, 119–188, DOI: 10.1111/gcb.14904 (2020).

11. Jackson, R. B., Mooney, H. A. & Schulze, E. D. A global budget for fine root biomass, surface area, and nutrient contents. *Proc. Natl. Acad. Sci. United States Am.* **94**, 7362–7366, DOI: 10.1073/pnas.94.14.7362 (1997).

12. Jackson, R. B. *et al.* A global analysis of root distributions for terrestrial biomes, DOI: 10.1007/BF00333714 (1996).

13. Bonan, G. *Climate Change and Terrestrial Ecosystem Modeling* (Cambridge University Press, 2019).

14. Taylor, K. E. Summarizing multiple aspects of model performance in a single diagram. *J. Geophys. Res. Atmospheres* **106**, 7183–7192, DOI: 10.1029/2000JD900719 (2001).

15. Bonan, G. B. *et al.* Modeling canopy-induced turbulence in the Earth system: a unified parameterization of turbulent exchange within plant canopies and the roughness sublayer (CLM-ml v0). *Geosci. Model. Dev* **11**, 1467–1496, DOI: 10.5194/gmd-11-1467-2018 (2018).

16. Oleson, K. W. *et al.* Technical Description of the version 5.0 of the Community Land Model (CLM). Tech. Rep. (2018).

17. Goudriaan, J. & Laar, H. H. v. *Modelling potential crop growth processes : textbook with exercises* (1994).

18. Sellers, P. J. Canopy reflectance, photosynthesis and transpiration. *Int. J. Remote. Sens.* DOI: 10.1080/01431168508948283 (1985).

19. Kowalczyk, E. A. *et al.* The land surface model component of ACCESS: description and impact on the simulated surface climatology. Tech. Rep. (2013).

20. De Pury, D. G. & Farquhar, G. D. Simple scaling of photosynthesis from leaves to canopies without the errors of big-leaf models. *Plant, Cell Environ.* **20**, 537–557, DOI: 10.1111/j.1365-3040.1997.00094.x (1997).

21. Goudriaan, J. *Crop micrometeorology: a simulation study*. Ph.D. thesis, Wageningen (1977).

22. Dai, Y. *et al.* A Two-Big-Leaf Model for Canopy Temperature, Photosynthesis, and Stomatal Conductance. *J. Clim.* **17**, 2281–2299, DOI: 10.1175/1520-0442(2004)017<2281:ATMFCT>2.0.CO;2 (2004).

23. Brutsaert, W. *Evaporation into the Atmosphere: Theory, History and Applications* (Kluwer Academic Publishers, 1982).

24. Monteith, J. & Unsworth, M. *Principles of Environmental Physics: Plants, Animals, and the Atmosphere: Fourth Edition* (2013).

25. Oleson, K. W. *et al.* Technical Description of version 4.5 of the Community Land Model (CLM). Tech. Rep., National Center for Atmospheric Research (2013). DOI: 10.5065/D6RR1W7M.

26. Medlyn, B. E. *et al.* Reconciling the optimal and empirical approaches to modelling stomatal conductance. *Glob. Chang. Biol.* **17**, 2134–2144, DOI: 10.1111/j.1365-2486.2010.02375.x (2011).

27. Farquhar, G. D., von Caemmerer, S. & Berry, J. A. A biochemical model of photosynthetic CO2 assimilation in leaves of C3 species. *Planta* DOI: 10.1007/BF00386231 (1980).

28. Damour, G., Simonneau, T., Cochard, H. & Urban, L. An overview of models of stomatal conductance at the leaf level. *Plant, Cell Environ.* **33**, 1419–1438, DOI: 10.1111/j.1365-3040.2010.02181.x (2010).

29. Campbell, G. S. & Norman, J. M. *An Introduction to Environmental Biophysics-Second Edition-* (1998).

30. Collatz, G., Ball, J., Grivet, C. & Berry, J. A. Physiological and environmental regulation of stomatal conductance, photosynthesis and transpiration: a model that includes a laminar boundary layer. *Agric. For. Meteorol.* **54**, 107–136, DOI: 10.1016/0168-1923(91)90002-8 (1991).

31. Bernacchi, C. J., Singsaas, E. L., Pimentel, C., Portis Jr, A. R. & Long, S. P. Improved temperature response functions for models of Rubisco-limited photosynthesis. *Plant, Cell Environ.* **24**, 253–259, DOI: 10.1111/j.1365-3040.2001.00668.x (2001).

32. Leuning, R. Temperature dependence of two parameters in a photosynthesis model. *Plant, Cell Environ.* **25**, 1205–1210, DOI: 10.1046/j.1365-3040.2002.00898.x (2002).

33. BERNACCHI, C. J., PIMENTEL, C. & LONG, S. P. In vivo temperature response functions of parameters required to model RuBP-limited photosynthesis. *Plant, Cell Environ.* **26**, 1419–1430, DOI: 10.1046/j.0016-8025.2003.01050.x (2003).

34. Hirose, T. & Werger, M. J. A. Maximizing daily canopy photosynthesis with respect to the leaf nitrogen allocation pattern in the canopy. *Oecologia* **72**, 520–526, DOI: 10.1007/BF00378977 (1987).

35. Wang, Y.-P. & Leuning, R. A two-leaf model for canopy conductance, photosynthesis and partitioning of available energy I: Model description and comparison with a multi-layered model. *Agric. For. Meteorol.* **91**, 89–111 (1998).

36. Kennedy, D. *et al.* Implementing Plant Hydraulics in the Community Land Model, Version 5. *J. Adv. Model. Earth Syst.* **11**, 485–513, DOI: 10.1029/2018MS001500 (2019).

37. Feng, X. *et al.* The ecohydrological context of drought and classification of plant responses. *Ecol. Lett.* **N/A**, 14, DOI: 10.1111/ele.13139 (2018).

38. Daly, E. *et al.* Coupled Dynamics of Photosynthesis, Transpiration, and Soil Water Balance. Part I: Upscaling from Hourly to Daily Level. *J. Hydrometeorol.* **5**, 546–558, DOI: 10.1175/1525-7541(2004)005<0546:CDOPTA>2.0.CO;2 (2004).

39. Pammenter, N. W. & Willigen, C. V. A mathematical and statistical analysis of the curves illustrating vulnerability of xylem to cavitation. In *Tree Physiology*, DOI: 10.1093/treephys/18.8-9.589 (1998).

40. Sperry, J. S., Adler, F. R., Campbell, G. S. & Comstock, J. P. Limitation of plant water use by rhizosphere and xylem conductance: Results from a model. *Plant, Cell Environ.* **21**, 347–359, DOI: 10.1046/j.1365-3040.1998.00287.x (1998).

41. Law, B. E. AmeriFlux US-Me2 Metolius mature ponderosa pine, Dataset. (2002).

42. Schwarz, P. A. *et al.* Climatic versus biotic constraints on carbon and water fluxes in seasonally drought-affected ponderosa pine ecosystems. *Glob. Biogeochem. Cycles* **18**, 1–17, DOI: 10.1029/2004GB002234 (2004).